The Astrophysical Journal, 988:110 (15pp), 2025 July 20 https://doi.org/10.3847/1538-4357/ade2e1

The Emerging Black Hole Mass Function in the High-redshift Universe

Junehyoung Jeon[1], Boyuan Liu[2], Anthony J. Taylor[1], Vasily Kokorev[1], John Chisholm[1], Dale D. Kocevski[3], Steven L. Finkelstein[1], and Volker Bromm[1,4]
[1] Department of Astronomy, University of Texas, Austin, TX 78712, USA; junehyoungjeon@utexas.edu
[2] Institut für Theoretische Astrophysik, Zentrum für Astronomie, Universität Heidelberg, D-69120 Heidelberg, Germany
[3] Department of Physics and Astronomy, Colby College, Waterville, ME 04901, USA
[4] Weinberg Institute for Theoretical Physics, University of Texas, Austin, TX 78712, USA
Received 2025 March 18; revised 2025 May 20; accepted 2025 June 6; published 2025 July 17

Abstract

Observations with the James Webb Space Telescope (JWST) have identified an abundant population of supermassive black holes (SMBHs) already in place during the first few hundred million years of cosmic history. Most of them appear overmassive relative to the stellar mass in their host systems, challenging models of early black hole seeding and growth. Multiple pathways exist to explain their formation, including heavy seeds formed from direct collapse/supermassive stars or sustained super-Eddington accretion onto light stellar remnant seeds. We use the semianalytical code Ancient Stars and Local Observables by Tracing Halos to predict the emerging SMBH mass function under physically motivated models for both light- and heavy-seed formation, to be compared with upcoming ultradeep JWST surveys. We find that both pathways can reproduce observations at $z \sim 5$–6, but have distinct features at higher redshifts of $z \sim 10$. Specifically, JWST observations have the potential to constrain the fraction of efficiently accreting (super-Eddington) SMBHs, as well as the existence and prevalence of heavy seeds, in particular through ultradeep observations of blank fields and/or gravitational lensing surveys. Such observations will provide key insights to understand the process of SMBH formation and evolution during the emergence of the first galaxies. We further emphasize the great promise of possible SMBH detections at $z \gtrsim 15$ with future JWST observations to break the degeneracy between light- and heavy-seed models.

Unified Astronomy Thesaurus concepts: Early universe (435); Galaxy formation (595); Supermassive black holes (1663); Active galactic nuclei (16); Theoretical models (2107)

1. Introduction

It has been firmly established that most galaxies in the local Universe host a supermassive black hole (SMBH) at their centers (e.g., J. Kormendy & L. C. Ho 2013). SMBHs are also known to accrete baryonic material from their vicinity and produce large amounts of radiation as active galactic nuclei (AGN; T. M. Heckman & P. N. Best 2014; R. C. Hickox & D. M. Alexander 2018). The seeds of SMBHs are expected to have formed at earlier times, subsequently evolving through accretion, feedback, and merger processes to produce the local correlations seen today between the SMBHs and the stellar properties of their host galaxies (e.g., K. Gebhardt et al. 2000; A. W. Graham et al. 2011; A. Beifiori et al. 2012; D. J. Croton 2006; X. Ding et al. 2020). To understand such coevolution, observations of SMBHs at high redshifts are crucial, and with the launch of the James Webb Space Telescope (JWST) a multitude of new AGN at $z \sim 3$–10 have been discovered (e.g., X. Ding et al. 2022; Á. Bogdán et al. 2024; I. Juodžbalis et al. 2023; D. D. Kocevski et al. 2023, 2025; V. Kokorev et al. 2023; R. L. Larson et al. 2023; M. Onoue et al. 2023; S. E. I. Bosman et al. 2024; S. Fujimoto et al. 2024; L. J. Furtak et al. 2024; J. E. Greene et al. 2024; R. Maiolino et al. 2024c; J. Matthee et al. 2024; A. J. Taylor et al. 2025).

These high-redshift SMBHs pose key questions: how did such massive objects form so early in cosmic history (e.g., A. Smith & V. Bromm 2019; T. E. Woods et al. 2019; K. Inayoshi et al. 2020)? The challenge to explain the emergence of quasars with large black hole (BH) masses ($\log M_{\rm BH}/M_{\odot} > 8$) at $z \gtrsim 6$ (X.-B. Wu et al. 2015; E. Bañados et al. 2018; K. Zubovas & A. King 2021; X. Fan et al. 2023) has been accentuated further with the recent JWST observations of AGN at even higher redshifts (e.g., R. L. Larson et al. 2023; L. J. Furtak et al. 2024; J. E. Greene et al. 2024). Of particular interest is the newly discovered, ubiquitous population of compact and highly dust-obscured objects, dubbed Little Red Dots (LRDs), that was unnoticed before JWST (D. D. Kocevski et al. 2023, 2025; H. B. Akins et al. 2024; J. Matthee et al. 2024). One possible explanation for the physical nature of these objects is that their rest-frame optical emission is powered by dust-obscured AGN (E. Durodola et al. 2025; H.-L. Huang et al. 2024; V. Kokorev et al. 2024). Other scenarios, such as extremely dense stellar clusters, have also been proposed to explain LRDs (J. F. W. Baggen et al. 2024; C. A. Guia et al. 2024; G. C. K. Leung et al. 2024; P. G. Pérez-González et al. 2024). Surprisingly, the vast majority of newly discovered high-z AGN are X-ray weak (with a few exceptions; e.g., D. D. Kocevski et al. 2025), with only upper limits established so far, which is in stark contrast to lower-redshift AGN and quasars (e.g., F. Pacucci & R. Narayan 2024; A. King 2025). Furthermore, many JWST-discovered AGN exhibit "overmassive" configurations, where the SMBH-to-galaxy stellar mass ratio is much higher than in the local Universe, subject to uncertainties in mass

measurement methodology (e.g., Á. Bogdán et al. 2024; V. Kokorev et al. 2023; F. Pacucci et al. 2023; P. Natarajan et al. 2024). This raises the question of whether the stellar system or the SMBH formed first, and how the two components affected each other through their respective feedback, eventually establishing the local correlations (e.g., B. Liu & V. Bromm 2022, 2023; V. Kokorev et al. 2024; J. Silk et al. 2024).

Two main formation channels have been suggested to address the aforementioned observations of massive SMBHs and overmassive systems at high redshift (L. Haemmerlé et al. 2020; K. Inayoshi et al. 2020; F. Sassano et al. 2021; M. Volonteri et al. 2021; J. Regan & M. Volonteri 2024): The first invokes "light-seed" remnant BHs, originating from the death of the first, metal-free, Population III (Pop III) stars (P. Madau & M. J. Rees 2001; A. Heger et al. 2003). Lacking any efficient metal cooling in the primordial clouds, Pop III stars are predicted to have a top-heavy initial mass function (IMF; e.g., A. Stacy et al. 2016; S. Hirano & V. Bromm 2017; M. A. Latif et al. 2022), resulting in more massive BH remnants ($\sim 10^2$–10^3 $M_\odot$) compared to local stellar remnant BHs. After formation, such Pop III seed BHs will grow further through accretion and mergers (M. Jeon et al. 2012; B. D. Smith et al. 2018; A. Trinca et al. 2022; A. K. Bhowmick et al. 2024a; A. J. Porras-Valverde et al. 2025).

The second, possibly less frequent, channel postulates "heavy-seed" direct-collapse BHs (DCBHs), formed from the collapse of a massive extremely metal-poor ($Z \lesssim 10^{-3}$ $Z_\odot$; S. Chon & K. Omukai 2025) gas cloud, involving a supermassive star as an intermediate, short-lived stage (e.g., V. Bromm & A. Loeb 2003; M. C. Begelman et al. 2006; G. Lodato & P. Natarajan 2006). This scenario, with a larger initial BH seed mass ($\sim 10^4$–10^6 $M_\odot$), relies on the rare conditions that prohibit gas cooling mechanisms at low temperatures to allow the cloud to collapse without fragmenting to form multiple stars (e.g., G. Lodato & P. Natarajan 2007; J. L. Johnson et al. 2013; L. Haemmerlé et al. 2018, 2020; J. H. Wise et al. 2019; Y. Luo et al. 2020). Alternatively, even if fragmentation is not completely avoided, heavy BH seeds can also form through runaway collisions of (proto-)stars or BHs in dense stellar clusters with high gas inflow rates and rapid accretion flows (R. S. Klessen & S. C. O. Glover 2023; B. Reinoso et al. 2023; L. Zwick et al. 2023; B. Gaete et al. 2024). Starting with a larger initial mass, such DCBH seeds may be subject to weaker timing constraints in growing to the observed high-z SMBH masses (e.g., Z. Haiman & A. Loeb 2001). Furthermore, the heavy-seed channel could naturally explain the inferred overmassive systems by forming a massive SMBH in an environment with initially few stars (E. Durodola et al. 2025; J. Jeon et al. 2025).

After BH seed formation, there are different scenarios for their growth to become the observed massive AGN. The theoretical maximum AGN luminosity is the Eddington limit, with a corresponding fiducial accretion rate that depends on the physics of the accretion flow (M. C. Begelman 1979). The light-seed channel under Eddington-limited growth cannot produce the observations of some of the most massive high-redshift AGN observations, due to ineffective growth over extended periods from stellar feedback that is heating the gas and the wandering movements of the central BH (J. L. Johnson & V. Bromm 2007; M. Milosavljević et al. 2009; J. Jeon et al. 2022; C. Partmann et al. 2025). Heavy-seed channels, on the other hand, can reach the inferred SMBH masses, as they operate in environments with less prominent stellar components, with more stationary SMBHs due to their larger initial masses (Y. Li et al. 2007; K. Inayoshi et al. 2020; R. L. Larson et al. 2023; J. Jeon et al. 2025). However, as the Eddington limit assumes spherical accretion, super-Eddington accretion rates are possible, at least for extended periods, via geometrically thick disk accretion modes (Y.-F. Jiang et al. 2014, 2019b; S. W. Davis & A. Tchekhovskoy 2020; M. Safarzadeh & Z. Haiman 2020). Invoking such super-Eddington accretion, the light-seed channel could also give rise to the high-redshift SMBHs, possibly providing a natural explanation for the unusual X-ray weakness of the AGN observed by JWST (e.g., R. Maiolino et al. 2025), including the LRDs (K. Inayoshi et al. 2024; P. Madau & F. Haardt 2024; F. Pacucci & R. Narayan 2024; K. Inayoshi 2025; A. King 2025).

To distinguish between the possible pathways toward the first SMBHs, further observations are needed that reach higher redshifts, supported by targeted theoretical predictions to interpret the observations. The heavy-seed model in particular can be independently tested with gravitational-wave (GW) detections of merging SMBH binaries with the Laser Interferometer Space Antenna (LISA; T. Robson et al. 2019), capable of accessing the required low-frequency regime (e.g., B. Liu & V. Bromm 2020a). Moreover, pulsar timing arrays (PTAs) have found evidence for a stochastic gravitational wave background (GWB; G. Agazie et al. 2023a; EPTA Collaboration et al. 2023; D. J. Reardon et al. 2023; H. Xu et al. 2023), which could be partially sourced by binary SMBHs (G. Hobbs & S. Dai 2017; J. D. Romano & N. J. Cornish 2017). However, the PTA constraints on the SMBH population are currently weak due to the high noise of the initial GWB data (e.g., G. Agazie et al. 2023b, 2023c).

In principle, the BH mass function (BHMF) at high z could be a powerful probe to disentangle distinct seeding models. A. J. Taylor et al. (2025) recently measured the broad-line AGN (BLAGN) BHMF over a wide dynamic range of BH masses for the first time at $z \sim 5$. However, comparing to models with a variety of seeding and growth mechanisms, they found that multiple models were consistent with the observations. They concluded that by $z \sim 5$, the "memory" of BH seeding is lost, and that BHMF measurements at higher redshifts (closer to the BH origin epoch) are needed.

Therefore, in this work, we aim to study the population statistics of even higher-redshift SMBHs, providing predictions for the evolving mass function and their hosts at $z \gtrsim 9$ under different SMBH evolution scenarios. We specifically utilize the semianalytical model (SAM) Ancient Stars and Local Observables by Tracing Halos (A-SLOTH; T. Hartwig et al. 2022, 2024; M. Magg et al. 2022), which models the formation and evolution of the first stars and is tuned to high-redshift constraints. We develop SMBH/AGN formation and growth models to be used in the A-SLOTH framework to study the coevolution of the SMBH, stellar, and halo populations. A-SLOTH is highly efficient and parallelized so that different SMBH scenarios can be rapidly tested and compared. Unlike previous works, we use an SAM focused on the high-redshift regime that models the formation of the first stars so that the first BH formation and evolution in the early Universe can be more accurately followed.

This paper is organized as follows. In Section 2, we introduce A-SLOTH, its relevant features, and the SMBH models we have developed. We present our predictions for

different SMBH evolution scenarios and their differences in Section 3. In Section 4 we discuss our results in the context of overall SMBH evolution at high redshifts and assess the prospects for future SMBH observations. We summarize our findings in Section 5.

2. Methodology

2.1. A-SLOTH

A-SLOTH is a semianalytical framework to model high-redshift galaxy formation, based on halo merger trees from *N*-body simulations or the extended Press–Schechter (EPS) formalism (H. Parkinson et al. 2008). The code has been calibrated to well reproduce the cosmic star formation (SF) rate density at $z \sim 4.5$–13.3 (T. Hartwig et al. 2024). We here employ the EPS approach, utilizing its computational speed to explore a broad parameter space. Within the provided merger tree, A-SLOTH models the formation and evolution of stellar populations and their effects on the cosmic environment. A-SLOTH uses an adaptive time step to trace halo evolution, which may be smaller than the time between two levels in the underlying tree. This time step is set to be a small fraction of the minimum between the halo SF, accretion, dynamical, and merger tree timescales (see Section 2.4 in T. Hartwig et al. 2022), with a typical value around 0.01–0.5 Myr. Below, we briefly summarize the relevant SF model in A-SLOTH, as well as our code modifications made to model SMBH evolution, and refer the reader for full details to the public release papers (T. Hartwig et al. 2022; M. Magg et al. 2022), as well as to the previous implementations of nuclear star clusters (NSCs) and galactic dynamics in B. Liu et al. (2024b).

2.1.1. Star Formation

A-SLOTH sets a critical halo mass above which the gas in the halo is assumed to be able to rapidly cool, such that SF can occur. This critical mass is the minimum between the atomic-cooling threshold where the halo acquires a virial temperature of $T_{\rm vir} \geqslant 10^4$ K, and the molecular cooling threshold that depends on the large-scale streaming velocity of the baryons ($v_{\rm BC}$) as well as the global Lyman–Werner (LW) background defined as

$$J_{21,\rm global} = 10^{2-z/5}, \tag{1}$$

where the background is given in units of J_{21} or 10^{-21} erg s^{-1} cm^{-2} Hz^{-1} sr^{-1} (T. H. Greif & V. Bromm 2006; T. Hartwig et al. 2022). The critical halo mass for efficient molecular cooling is (A. T. P. Schauer et al. 2021)

$$\log_{10}(M_{\rm crit}/M_\odot) = 6.02(1.0 + 0.17\sqrt{J_{21}}) + 0.42 v_{\rm BC}. \tag{2}$$

If the halo mass exceeds either of the critical mass values, it is considered for SF. T. Hartwig et al. (2022) chose $v_{\rm BC} = 0.8$ as the most probable value (A. T. P. Schauer et al. 2019), for which the two masses are equal at $z \lesssim 10$, also used here as our default parameter choice. The $v_{\rm BC}$ value is normalized by the rms streaming velocity at recombination, $\sigma_{\rm rms} \simeq 30$ km s^{-1} (A. T. P. Schauer et al. 2021). However, in reality, there is a distribution of the streaming velocity $v_{\rm BC}$ encountered by the dark matter (DM) halos. Therefore, we also test two other $v_{\rm BC}$ values, zero and two, and create a secondary model from the weighted mean of the three runs with these three $v_{\rm BC}$ values. The weighted mean is determined from the probability distribution of $v_{\rm BC}$ (B. Liu et al. 2024a).

When a halo forms stars, if the halo metallicity is below a critical value, the first generation of metal-free stars (Pop III) will be formed and if the metallicity is above the critical value, the second generation of metal-enriched stars (Population II (Pop II)) will be formed. This critical metallicity is defined as

$$10^{[\rm C/H]-2.30} + 10^{[\rm Fe/H]} > 10^{-5.07}, \tag{3}$$

where [Fe/H] and [C/H] are the iron and carbon abundances of the star-forming gas such that when this condition is met, Pop II stars will form (G. Chiaki et al. 2017). Furthermore, A-SLOTH divides the baryonic material in the halo into four components: cold gas, hot gas, stars, and outflows, where only the cold gas contributes to SF. The newly formed stellar population is assigned a mass based on the cold gas properties according to

$$M_*^i = \eta_* M_{\rm cold}^i \frac{\delta t_i}{t_{\rm cold,ff}^i}, \tag{4}$$

where i is the time step index, $M_{\rm cold}$ is the cold gas mass of the halo, $t_{\rm cold,ff}$ is the corresponding freefall time, δt is the time step, and η_* is the SF efficiency (SFE). The SFE has been calibrated in T. Hartwig et al. (2024) to have best-fit values of 8.15 for Pop III and 0.237 for Pop II stars. The SFE can be greater than one as it is defined as the fraction of cold gas that is converted into stars per freefall time for the average cold gas density. An SFE larger than one thus represents the case when the SF timescale is shorter than the average freefall time. The average number of stars is computed in logarithmically spaced IMF bins, which are used to draw individual stars with Poisson sampling. For Pop II, the Kroupa IMF (P. Kroupa 2001) is used and for Pop III, a power-law IMF of

$$\frac{dN}{d\log M_{\rm star}} \propto M_{\rm star}^{-1}, \tag{5}$$

is used. The Pop III component has a stellar lifetime based on the fitting function (D. Schaerer 2002)

$$\log_{10}(t_{\rm III}/{\rm yr}) = 9.785 - 3.759x + 1.413x^2 - 0.186x^2, \tag{6}$$

whereas for Pop II, the lifetime is expressed as (S. W. Stahler & F. Palla 2004)

$$\log_{10}(t_{\rm II}/{\rm yr}) = 10 - 3.68x + 1.17x^2 - 0.12x^3, \tag{7}$$

where $x = \log_{10}(M_{\rm star}/M_\odot)$ and $M_{\rm star}$ is the individual stellar mass.

2.1.2. Photo-heating Feedback

Photo-heating feedback from massive stars ($>5\ M_\odot$) can convert the cold gas in halos to hot gas. The instantaneous conversion rate is estimated assuming the L. Spitzer (1978) solution for the H II region expansion from stellar photo-ionization as

$$\dot{M}_{\rm heat} = m_{\rm H} n_{\rm cold} R_{\rm St}^2 c_{s,\rm ion} \left[1 + \frac{7}{4}\frac{c_{s,\rm ion}(t - t_{\rm St})}{R_{\rm St}}\right]^{-1/7}, \tag{8}$$

where $m_{\rm H}$ is the hydrogen mass, $n_{\rm cold} = 10^3$ cm^{-3} is the neutral gas number density around a newly formed star, $R_{\rm St}$ is the Strömgren radius, t is the time, $t_{\rm St}$ is the time the ionization front reaches $R_{\rm St}$, and $c_{s,\rm ion}$ is the sound speed of the ionized gas at 10^4 K.

A-SLOTH assumes that 90% of massive stars in a halo form inside one cluster at the galactic center, whereas the other 10% of massive stars form in isolation (L.-H. Chen et al. 2022). As regions of heating overlap for star clusters, they heat up their environment less efficiently compared to isolated stars. Therefore, the ionizing photons from 90% of massive stars are combined to compute one mass conversion rate for the star cluster and individual rates are computed for isolated stars. In a time step dt, the total gas mass heating rate from massive stars is thus given by

$$\delta M_{\rm heat} = \left(\dot{M}_{\rm heat,cluster} + \sum_{j=1}^{0.1N} \langle \dot{M}^{j}_{\rm heat,isolated} \rangle \right) dt\,, \tag{9}$$

where N is the number of massive stars.

2.1.3. Supernova Feedback

After a stellar lifetime has passed, if the star's mass is in the range 10–40 $M_\odot$, it will explode as a core-collapse supernova (SN), and if a Pop III star is in the mass range 140–260 $M_\odot$, it will explode as a pair-instability SN. The energies produced by these events are shown in Figure 2 of T. Hartwig et al. (2022). The feedback from SNe is implemented as gas ejections from the halo by comparing the gas binding energy to the SN feedback energy, where the former has contributions from DM, cold and hot gas, as well as stars. Specifically, the hot and cold gas binding energies at step i are defined as

$$E^{i}_{\rm bind,hot} = \frac{G M_{\rm vir,peak} M_{{\rm hot},i}}{R_{\rm vir}} \chi_{\rm hot,1} + \chi_{\rm hot,2}, \tag{10}$$

$$E^{i}_{\rm bind,cold} = \frac{G M_{\rm vir,peak} M_{{\rm cold},i}}{R_{\rm vir}} \chi_{\rm cold,1} + \chi_{\rm cold,2}, \tag{11}$$

where $M_{\rm vir,peak}$ is the peak halo virial mass, $R_{\rm vir}$ is the halo virial radius, $M_{\rm hot,cold}$ is the hot/cold gas mass, and $\chi_{\rm (hot,cold),(1,2)}$ are factors accounting for the binding energy arising from the DM, the hot/cold gas disk, and the stellar disk (L.-H. Chen et al. 2022). Full expressions and derivations for these binding energies can be found in L.-H. Chen et al. (2022) and T. Hartwig et al. (2022).

The total SN energy at each step i, $E^{i}_{\rm SNe}$, is distributed to some fractions of hot and cold gas, depending on the respective binding energies as

$$f_{\rm hot} = \frac{E^{i}_{\rm bind,hot} M^{i}_{\rm hot}}{E^{i}_{\rm bind,hot} M^{i}_{\rm hot} + E^{i}_{\rm bind,cold} M^{i}_{\rm cold}}, \tag{12}$$

$$f_{\rm cold} = \frac{E^{i}_{\rm bind,cold} M^{i}_{\rm cold}}{E^{i}_{\rm bind,hot} M^{i}_{\rm hot} + E^{i}_{\rm bind,cold} M^{i}_{\rm cold}}. \tag{13}$$

Furthermore, we adopt an outflow efficiency $\gamma_{\rm out}$, defined as (L.-H. Chen et al. 2022)

$$\gamma_{\rm out} = \left(\frac{M_{\rm vir,peak}}{M_{\rm out,norm}} \right)^{\alpha_{\rm out}}. \tag{14}$$

The normalization mass, $M_{\rm out,norm}$, and $\alpha_{\rm out}$ are free parameters calibrated in T. Hartwig et al. (2024) so that for the same SN energy, relatively more gas is removed from less massive halos than more massive ones.

Overall, the amount of hot/cold gas ejected by SNe is determined as the ratio between the SN energy and the gas binding energy, accounting for the outflow efficiency and the fraction of gas to be affected, according to

$$\delta M^{i}_{\rm out,(hot,cold)} = \min\left(\frac{E^{i}_{\rm SNe} f_{\rm (hot,cold)} / \gamma_{\rm out}}{E_{\rm bind,(hot,cold)}} M^{i}_{\rm (hot,cold)},\, M^{i}_{\rm (hot,cold)} \right). \tag{15}$$

The SN metal yields are taken from the tabulation in K. Nomoto et al. (2013) for Pop III and C. Kobayashi et al. (2006) for Pop II stars.

2.2. Black Hole Seeding

We consider two classes of BH seeds, light ones originating from Pop III stellar remnants ($\sim$100 $M_\odot$) and heavy DCBH seeds from collapsing massive clouds/supermassive stars ($\sim 10^5$ $M_\odot$). Our specific process of assigning BH seeds to halos is as follows.

Each halo in the merger tree is checked to see if any of the halo's progenitors hosted a BH already. If no progenitors hosted a BH or if the halo is the very first progenitor, we assess the halo conditions and determine whether it should be seeded with a BH. When a massive (>40 $M_\odot$) Pop III star in the halo dies and its mass is outside the core-collapse or pair-instability SN range, 40 $M_\odot < M_* <$ 140 $M_\odot$ or $M_* >$ 260 $M_\odot$, respectively, a light seed of the same mass as the dying Pop III star is assigned at the halo center. We do not consider Pop II stars for simplicity and as they will result in much lower-mass BHs ($\sim$5–10 $M_\odot$) compared to the more massive Pop III remnants (A. Stacy et al. 2016; F. Sassano et al. 2021; M. Volonteri et al. 2021; M. A. Latif et al. 2022).

For heavy seeds, we consider a set of criteria based on the halo virial temperature, metallicity, and LW feedback to capture the dense, hot, and metal-poor conditions required for DCBH formation and ensure that the gas in the halo is not able to cool and fragment too quickly to form regular stars instead (V. Bromm & A. Loeb 2003; K. Ardaneh et al. 2018; J. H. Wise et al. 2019; S. Chon et al. 2021). Specifically, we require that the virial temperature of the halo be greater than 10^4 K, above the atomic-cooling limit, to be able to host gas that can collapse (nearly) isothermally, even in the absence of H_2 cooling. We further impose that the metallicity of the star-forming gas in the halo be smaller than a critical metallicity, $Z < Z_{\rm crit} = 2 \times 10^{-4}\, Z_\odot$ (B. Liu & V. Bromm 2020a) to not allow for too efficient metal cooling. Recent work has shown that heavy seeds could form even at higher metallicities up to 10^{-3} $Z_\odot$ (S. Chon & K. Omukai 2025). We have tested this higher-metallicity threshold, and found that while around 50% more heavy seeds do form, they are still subdominant to the overall BH population and do not significantly affect our results especially at higher redshifts. Thus, we adopt the default critical value of 2×10^{-4} $Z_\odot$ throughout the paper. Finally, we impose that the LW background in the halo be greater than the critical level, $J_{\rm LW} > J_{\rm crit}$, so that LW radiation can dissociate H_2 and disable molecular cooling, thus preventing SF.

Table 1
Summary of Model Parameters

Name	BH Seeding	Accretion Mode	$f_{\rm Edd}$	$f_{\rm duty}$
Light seeds forced super-Eddington	Light only	Eddington	1.5	0.8
Light seeds super-Eddington limited	Light only	Bondi	1.5	0.5
Heavy seeds Eddington limited	Heavy and Light	Bondi	1	0.5
Heavy seeds super-Eddington limited	Heavy and Light	Bondi	1.5	0.5
Heavy seeds forced super-Eddington	Heavy and Light	Eddington	1.5	0.5

Note. The heavy-seeds forced super-Eddington model is only used to probe the most extreme BH mass growths (see Figure 2), as it exceeds observations even more extremely than the light-seeds forced super-Eddington model (see Figure 1).

We set $J_{\rm crit} = 300$, in units of J_{21} (A. Trinca et al. 2022), and we consider both global and local LW contributions.[5] The global LW background is defined in Equation (1) above, and is generally subdominant relative to $J_{\rm crit}$, but we include it for completeness. The local LW flux within a given halo generally provides the main contribution to the LW radiation, and is calculated from considering massive stars, above 5 $M_\odot$, that are capable of producing LW radiation (11.2–13.6 eV) efficiently. We determine the LW photon production rate of each active massive stars based on the stellar mass from the fitting formula in Y. Deng et al. (2024, see their Equation (8)), further assuming for simplicity that the high-mass stars are located on average at 0.1 $R_{\rm vir}$ of the halo center. Thus, for a given halo, its LW flux is the sum of the global background and the local component, produced by the massive stars in the halo. Other studies have concluded that local LW radiation alone could not establish conditions for DCBH formation (J. Sullivan et al. 2025), as gas must initially cool below $\lesssim$1000 K to form stars first, and there is insufficient time to subsequently heat the gas up again to the atomic-cooling threshold. Our model represents the optimistic scenario where the local massive stars have formed in the progenitor halos, whose mergers heat the gas to $\sim 10^4$ K, triggering prompt DCBH formation within $\sim$1 Myr, before the gas reservoir is destroyed by feedback. If all the above criteria are met, regarding virial temperature, metallicity, and LW radiation, the halo is endowed at its center with a heavy seed of mass $10^5\ M_\odot$ (e.g., F. Becerra et al. 2018a, 2018b). The median cold gas mass in halos right after DCBH formation is $\sim 5 \times 10^4\ M_\odot$, of the same order as the initial DCBH mass, agreeing with the theoretical scenario that DCBH formation should take up most of the initially available cold gas in the host halo (J. H. Wise et al. 2019).

If any of the halo's progenitors contains a BH, the halo inherits at its center the one from the most massive progenitor host. If the most massive progenitor hosts multiple BHs, the other BHs are also inherited at their respective positions. If multiple progenitors host BHs, the BHs from the less massive progenitors are inherited as well, but placed at random (apocenter) distances from the halo center. In assigning distances, we follow the spatial distribution of Pop III remnants, derived from high-resolution simulations (B. Liu & V. Bromm 2020a, 2020b) for BHs with masses $M_{\rm BH} < 10^5\ M_\odot$, and the locations of NSCs after halo mergers found in previous A-SLOTH implementations (B. Liu et al. 2024b) for BHs with $M_{\rm BH} \geqslant 10^5\ M_\odot$. We have adopted the NSCs as tracers of postmerger massive BH locations, as NSCs are thought to reside in the centers of dwarf halos, similar to the massive BHs (A. Askar et al. 2023; N. Chen et al. 2024; C. Partmann et al. 2025). Finally, the BH orbits are assigned random eccentricities drawn from a uniform distribution in [0, 1) (B. Liu et al. 2024b).

[5] The physics behind the critical flux is complex and still rather uncertain (see, e.g., K. Sugimura et al. 2014). The resulting DCBH number density is thus very uncertain as well, varying with the critical level as $J_{\rm crit}^{-4}$ (e.g., K. Inayoshi & T. L. Tanaka 2015; S. Chon et al. 2016).

2.3. Two Models of Black Hole Accretion

At each time step, we update the BH mass and location through accretion and dynamical friction. These steps are crucial to be able to model BH evolution, but with the lack of information on the gas distribution near the BH in SAMs, it is difficult to estimate BH accretion. Therefore, we consider two models of BH accretion, Eddington and Bondi.

We constrain the accretion rate to be limited by the available cold gas mass in the halo as

$$\delta M_{\rm BH} = \min(f_{\rm duty}\dot{M}_{\rm acc}\,dt,\ M_{\rm cold}), \tag{16}$$

where $f_{\rm duty}$ is the duty cycle for active accretion onto the SMBH (F. Pacucci et al. 2023; S. Lai et al. 2024). Here, the duty cycle is a free parameter which we choose to reproduce existing observations (see Table 1). For the two models, we use different methods to determine the accretion rate $\dot{M}_{\rm acc}$.

In the Eddington mode, we use the fiducial physical upper limit of accretion, the Eddington rate, thus representing optimistic BH growth trajectories. More specifically, this rate is parameterized by the Eddington ratio $f_{\rm Edd}$ as

$$\dot{M}_{\rm Edd} = 2.7 \times 10^{-3} \left(\frac{M_{\rm BH}}{10^5\ M_\odot}\right)\left(\frac{\epsilon_r}{0.1}\right)^{-1} M_\odot\ {\rm yr}^{-1}, \tag{17}$$

such that

$$\dot{M}_{\rm acc} = f_{\rm Edd}\,\dot{M}_{\rm Edd}. \tag{18}$$

Here, $\epsilon_r = 0.1$ is the radiative efficiency, and we allow the Eddington ratio $f_{\rm Edd}$ to be larger than one, corresponding to super-Eddington accretion. We adjust this parameter to ensure that the resulting SMBH population agrees with the observed high-redshift BH mass function (see Section 3). The Eddington model, while positing that every BH will accrete at the same fraction, $f_{\rm Edd}$, of the Eddington rate, does not make assumptions about the gaseous environment near the BH, and is mainly dependent on the current BH mass.

We note that the radiative efficiency may be smaller (0.01–0.05) at earlier times, especially for super-Eddington cases (Y.-F. Jiang et al. 2014, 2019b). If so, the Eddington accretion rate of the SMBHs will be higher for a given mass, implying faster growth. However, the effect of lower ϵ_r can be similarly reproduced by adjusting $f_{\rm Edd}$ to a higher value, to a

more super-Eddington accretion. Thus, the choice of ϵ_r is not crucial within our modeling, as the consequence of super-Eddington accretion can be represented by other free parameters.

For the Bondi model, we use the Bondi–Hoyle formalism (H. Bondi & F. Hoyle 1944):

$$\dot{M}_{\rm Bondi} = \alpha \frac{4\pi (G M_{\rm BH})^2 \rho_g}{c_s^3}, \tag{19}$$

where ρ_g is the gas density, c_s is the sound speed, and α is the boost factor, which is a free parameter. The boost factor accounts for the enhanced gas density in the inner regions of the halo near the central BH that is not well captured in cosmological simulations (J. Jeon et al. 2022), or with idealized halo profile models (A. Trinca et al. 2022). We set it to unity in this work, given that A-SLOTH explicitly models the cold gas in the halo. For ρ_g, we consider only the cold gas mass $M_{\rm cold}$ as contributing to BH accretion, assuming that it is confined to within the halo scale radius, $R_s = R_{\rm vir}/c_{\rm DM}$, of the Navarro–Frenk–White (NFW) DM halo profile (J. F. Navarro et al. 1996), where $c_{\rm DM}$ is the halo concentration parameter (T. Hartwig et al. 2022). The DM concentration is given by the fitting functions from C. A. Correa et al. (2015). Thus, we approximate the cold gas density distribution as an isothermal sphere with a flat core (A. Trinca et al. 2022):

$$\rho(r) = \frac{\rho_{\rm norm}}{1 + (r/r_{\rm core})^2}, \tag{20}$$

where $r_{\rm core} = 0.012 R_{\rm vir}$ is the halo core radius (A. Trinca et al. 2022) and $\rho_{\rm norm}$ is the normalization density. The latter is set so that the integral of Equation (20) up to the scale radius R_s equals the total $M_{\rm cold}$.

We evaluate this expression at the Bondi radius of the BH, $r_b = G M_{\rm BH}/c_s^2$, where $c_s = \sqrt{k_{\rm B} T/m_g}$, with $k_{\rm B}$ being the Boltzmann constant, T is the gas temperature, and m_g is the mean molecular weight of the gas. To estimate the gas temperature in an idealized fashion, we use the halo viral temperature plus an effective contribution expressing the heating from BH feedback, $T_{\rm vir} + T_{\rm feed}$, when the average metallicity is below $Z_{\rm crit}$. If the latter is above $Z_{\rm crit}$, on the other hand, we employ the cold gas temperature at the given redshift plus the BH feedback contribution, $T_{\rm cold} + T_{\rm feed}$, reflecting the fact that at high redshifts, the cold gas in the halo should be able to efficiently cool to temperatures lower than the halo virial temperature. The cold gas temperature $T_{\rm cold}$ is set to the cosmic microwave background (CMB) temperature (e.g., C. Safranek-Shrader et al. 2016). Such cold gas near the CMB temperature has been found in high-resolution simulations even at lower redshifts $z \sim 5$–6 (B. Liu & V. Bromm 2020a; J. Jeon et al. 2023). We note that thus using the CMB temperature sets the upper bound on accretion.

The additional heating from BH feedback, expressed in the equivalent $T_{\rm feed}$, is described below (see Section 2.5). We further limit the accretion rate to a multiple of the Eddington value (Equation (17)) as

$$\dot{M}_{\rm acc} = \min(\dot{M}_{\rm Bondi}, f_{\rm Edd} \dot{M}_{\rm Edd}). \tag{21}$$

Compared to the Eddington model, the Bondi model has the advantage of adapting to the physical conditions in the vicinity of individual BHs. However, unlike for the Eddington model, idealized estimates have to be used for the cold gas density and temperature, as such information is not directly available in SAMs. Overall, the Eddington model proceeds with fewer assumptions, whereas the Bondi model represents a more physically realistic approach.

For both models, $\delta M_{\rm BH}$ is removed from the cold gas reservoir of the halo. Accretion is only applied to the primary BH, which is assumed to reside in the halo center, where the dense and cold gas is also located. The other BHs are assumed to not accrete for simplicity, in line with previous work showing that wandering BHs that do not reside in the dense central region generally do not accrete efficiently and thus remain dormant (J. Jeon et al. 2023; E. Ogata et al. 2024).

2.4. Black Hole Dynamics and Mergers

If a BH is not at the center of a halo after halo mergers, we follow its inspiral and update its location and eccentricity at each (SF) time step using the dynamical friction prescription from stars and DM in B. Liu et al. (2024b, their Equations (2)–(4)). Specifically, the change in distance from the center r and eccentricity e is modeled according to

$$\frac{dr}{dt} \simeq -r \left[\frac{1}{\tau_{{\rm DF},*}} + \frac{1}{\tau_{{\rm DF},\chi}} \right], \tag{22}$$

$$\frac{de}{dt} \simeq -e \left[\frac{1}{\tau_{{\rm DF},*}} + \frac{1}{\tau_{{\rm DF},\chi}} \right], \tag{23}$$

where $\tau_{{\rm DF},*}$ is the dynamical friction timescale arising from the halo stellar component, and $\tau_{{\rm DF},\chi}$ is that from the DM component. This timescale can be evaluated using the Chandrasekhar formula (J. Binney & S. Tremaine 2008):

$$\frac{\tau_{\rm DF}}{\rm Myr} = \frac{342}{\ln \Lambda} \left(\frac{r}{3\ {\rm pc}} \right)^2 \left(\frac{v}{10\ {\rm km\ s^{-1}}} \right) \left(\frac{M_{\rm BH}}{100\ M_\odot} \right)^{-1}, \tag{24}$$

where $\ln\Lambda$ is the Coulomb logarithm and v is the circular velocity. We use $\ln\Lambda \sim \ln[M_* r/(0.8 M_{\rm BH} R_*)]$ and $v \sim \sigma_* \sim \sqrt{G M_*/(0.8 R_*)}$ for $\tau_{{\rm DF},*}$, given the total stellar mass M_* and size R_* of the galaxy. The stellar parameters, M_* and R_*, are replaced with the virial mass and radius, $M_{\rm vir}$ and $R_{\rm vir}$, when calculating $\tau_{{\rm DF},\chi}$. When the inner slope of the density profile of the host galaxy is $0 < \gamma_* < 2$, as defined in M. Arca-Sedda et al. (2015) for a dwarf starburst galaxy, we use a generalization of the Chandrasekhar formula above for evaluating the stellar term. The analytical fit used is valid for both cored and cusped density profiles and generally produces smaller timescales than Equation (24) (B. Liu et al. 2024b). For a more complete description, we refer the reader to M. Arca-Sedda et al. (2015), M. Arca-Sedda (2016), and B. Liu et al. (2024b).

We introduce a merging radius, $r_{\rm merge}$, such that if a BH wanders inside the $r_{\rm merge}$ of the central BH, we assume that the two BHs have merged, updating the mass of the central BH accordingly and removing the merged BH from subsequent tracking. The merging radius is set to

$$r_{\rm merge} = \frac{G M_{\rm BH}}{v_{\rm vir}^2}, \tag{25}$$

where $v_{\rm vir}$ is the halo virial velocity. We note that here we ignore the delay time of BH mergers proceeding under GW emission, and the gravitational recoil after merger. Therefore, we explore the optimistic case where BH mergers occur efficiently and do not remove the product from the host galaxy.

2.5. Black Hole Feedback

We implement BH feedback as injection of thermal energy, resulting from BH accretion. More specifically, the energy injected to the nearby cold gas at each time step dt is

$$E_{\rm BH} = \epsilon_w \epsilon_r \dot{M}_{\rm BH} c^2 dt, \tag{26}$$

where $\dot{M}_{\rm BH}$ is the effective BH accretion rate, and $\epsilon_w = 0.02$ is the radiation–thermal coupling efficiency (M. Tremmel et al. 2017). This injected energy is converted to the increase in the gas temperature nearby the BH according to

$$T_{\rm feed} = (\gamma - 1)\frac{E_{\rm BH} m_g}{k_{\rm B} M_{\rm gas}}, \tag{27}$$

where $\gamma = 5/3$ is the polytropic index of the gas, and $M_{\rm gas}$ is the combined mass of the cold and hot gas in the halo. This temperature is used in determining the sound speed for the Bondi model in Equation (19) (see Section 2.3 above). We assume that the BH feedback does not significantly affect SF, as its impact is still quite uncertain. Some observations, for example, show no correlation between the SF rate and AGN activity (e.g., J. Scholtz et al. 2025; G. A. Oio et al. 2024; A. Suresh & M. R. Blanton 2024). Furthermore, the relatively lower-mass BHs expected at high redshifts imply an overall smaller effect on SF.

2.6. Cosmological Volume

To model a population of SMBHs in a cosmologically representative volume in EPS trees, we use the methodology in M. Magg et al. (2016). We run A-SLOTH for 300 halo masses at $z = 1$ between $M_{\rm halo,min} = 5 \times 10^8\, M_\odot$ and $M_{\rm halo,max} = 2 \times 10^{13}\, M_\odot$ at evenly spaced logarithmic mass bins. This range of halo masses was chosen so that the low-mass end of the merger tree will still contain Pop III star-forming halos and the upper mass end to include halos that are too rare to contribute significantly to a cosmologically representative sample, thus probing both the general population and extreme cases of SMBH formation and evolution. For each halo mass M_i, we define $M_{i,\rm up/down} = 0.5(M_i + M_{i\pm1})$. We then include the results of each run depending on the comoving halo number density of that mass at $z = 1$ with the weight

$$w_i = \frac{f_{\rm duty}}{M_i}\int_{M_{i,\rm down}}^{M_{i,\rm up}} \frac{dn}{d\ln M} dM, \tag{28}$$

where $dn/d\ln M$ is the halo mass function at $z = 1$, using the R. K. Sheth et al. (2001) halo mass function implemented in the Colossus package (B. Diemer 2018). The factor of $f_{\rm duty}$, the fraction of the time that SMBHs are accreting, is included to account for the fact that observations will only detect actively accreting SMBHs.

3. Results

We carry out a suite of runs with different sets of seeding and accretion models. For seeding, we consider two cases with heavy seeds included, and one where only light seeds form. For accretion, we explore the Eddington and Bondi models (see Section 2.3). As free parameters, we vary the Eddington ratio $f_{\rm Edd}$ and the accretion duty cycle $f_{\rm duty}$. We note that within the Eddington model, $f_{\rm Edd}$ determines the actual accretion rate for all BHs, while for the Bondi model, $f_{\rm Edd}$ sets the upper limit for accretion. We assign values to the free parameters so that the observed BH mass function at $z \sim 3.5$–6 can be reproduced (A. J. Taylor et al. 2025), or the highest-redshift AGN, at $z \sim 10$, can be explained (Á. Bogdán et al. 2024; R. Maiolino et al. 2024c). The full suite of models explored in this paper is summarized in Table 1. Regarding the effect of relative DM–baryon streaming, we specifically consider two sets of runs for each model, as described in Section 2.1.1: one with $v_{\rm BC} = 0.8$ for all halos, and the other with a weighted distribution of $v_{\rm BC}$ values.

3.1. Supermassive Black Hole Demographics

We first examine the overall demographics of the high-redshift BH population, arising from each model, and show how model parameters can be calibrated. In Figure 1, we show the resulting BHMF for all models at $z = 9$–10 and $z = 5$–6. We do not extend our models to $z \lesssim 5$ as A-SLOTH was calibrated against observational constraints for a cosmologically representative galaxy population only at high redshifts ($z > 4.5$; T. Hartwig et al. 2022, 2024).[6] The BHMF exhibits peaks at the BH seeding masses, at $\sim$100 $M_\odot$ for light seeds, and 10^5 $M_\odot$ for heavy seeds. The amplitude of the (heavy-seed) peak is very sensitive to the model parameters (see in particular Section 2.2 on the dependence on $J_{\rm crit}$), and we here probe the upper limit on heavy-seed (DCBH) abundance with our assumption for the strength of local LW sources. We specifically consider a model where the critical LW value for DCBH formation is increased to $J_{\rm crit} = 3000$ (with $v_{\rm BC} = 0.8$), which results in a much lower peak amplitude, thus demonstrating the strong dependence on the heavy-seed criteria. We note that the amplitude of the fiducial DCBH peak ($\sim$0.1–1 Mpc^{-3} dex^{-1}) is higher than locally inferred abundances for 10^6 $M_\odot$ SMBHs ($\sim 10^{-3}$–10^{-2} Mpc^{-3} dex^{-1}; A. Marconi et al. 2004; J. E. Greene et al. 2020). Such a large DCBH population could possibly be accounted for if many heavy seeds remained dormant and were not luminous, either through the effects of stellar feedback (J. Jeon et al. 2023) or dynamical wandering away from galaxy centers (M. Mezcua & H. Domínguez Sánchez 2020; A. E. Reines et al. 2020), thus rendering them undetectable with current observational facilities. Furthermore, our heavy-seeding model represents upper limits, in line with the conclusion in other works, invoking similarly optimistic scenarios that heavy seeds could account for all SMBHs in the Universe under these conditions (S. Chon & K. Omukai 2025). Lastly, the heavy-seed model had originally been introduced to explain the most massive SMBHs at early times, similar to the argument presented here that they are needed to account for the extremely massive

[6] Low-z constraints for Milky Way–like galaxies are also considered in the calibration of A-SLOTH. However, it is unknown if the calibration results can be applied to cosmological simulations at $z < 4.5$, since they may be biased by the specific assembly histories of Milky Way–like galaxies.

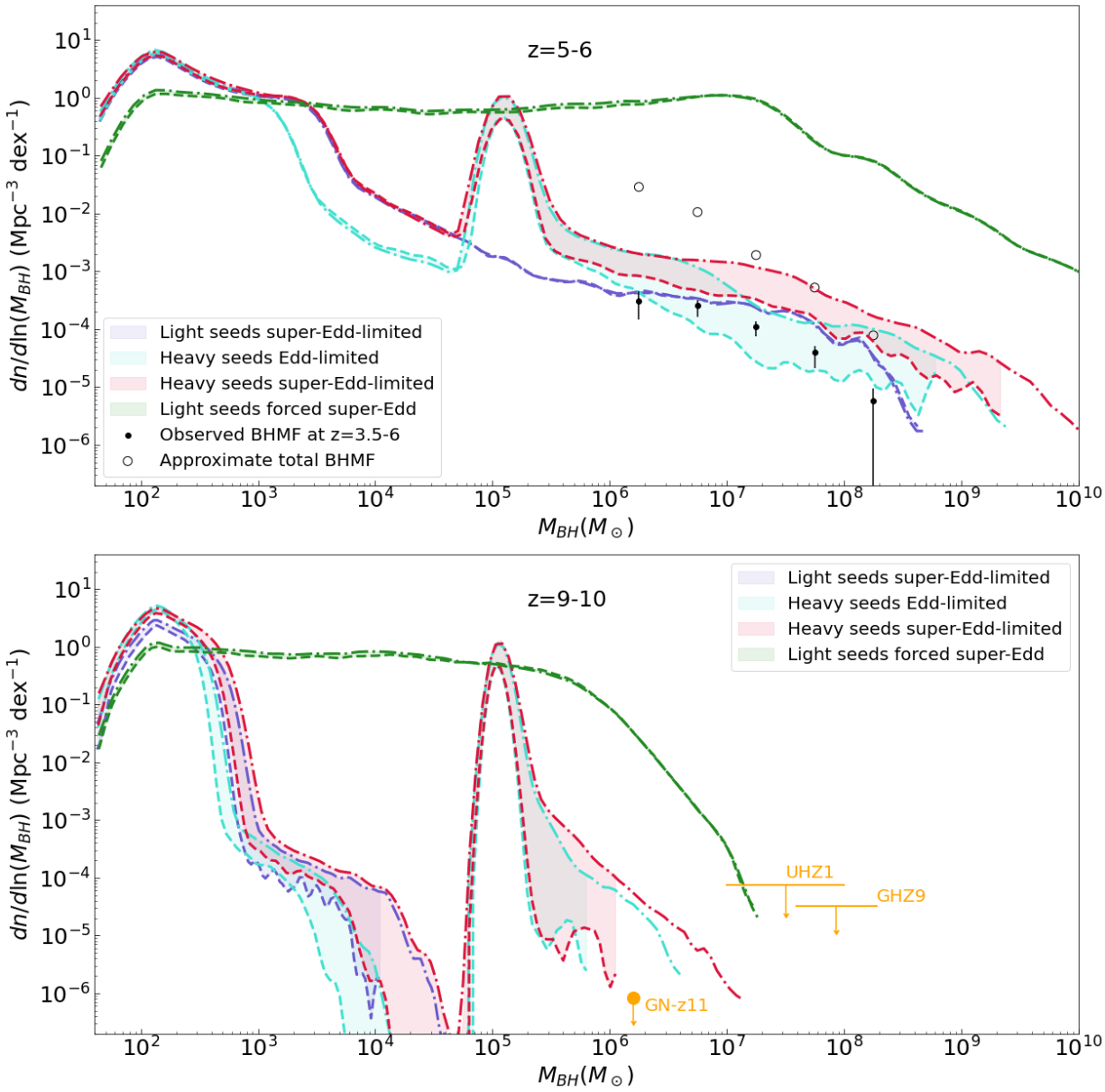

Figure 1. BHMF at $z = 5$–6 (top) and $z = 9$–10 (bottom), as predicted by our models. The default model with $v_{\rm BC} = 0.8$ is shown as dashed lines and the ensemble model from the weighted mean of runs with $v_{\rm BC} = 0$, 0.8, and 2 is shown with dotted–dashed lines. The change in the streaming velocity $v_{\rm BC}$ only significantly affects heavy-seed formation. We also show a model where the critical LW flux for DCBH formation is increased to $J_{\rm crit} = 3000$, to demonstrate that the peak amplitude for the heavy-seed models are strongly dependent on the model parameters. We compare our models against the observed BLAGN BHMF at $z = 3.5$–6 (J. Matthee et al. 2024; A. J. Taylor et al. 2025) and approximate upper limits derived from individual AGN observations at $z \sim 10$ (T. Treu et al. 2022; Á. Bogdán et al. 2024; L. J. Furtak et al. 2024; R. Maiolino et al. 2024c; L. Napolitano et al. 2024). As the observed BHMF is specifically targeting BLAGN, we also plot (open circles) the approximate total BHMF, which includes obscured and dormant SMBHs, based on the TRINITY model (H. Zhang et al. 2023). All models with Bondi accretion can approximately reproduce the observed BHMF. As the accretion duty cycle is a free parameter here, and can be set to a lower value, the super-Eddington-limited models represent the optimistic upper limit for the BHMF. However, only the forced super-Eddington model can reproduce the extreme UHZ1 system at $z = 10.1$, observed at a redshift comparable to the range modeled here. Therefore, while the overall SMBH/AGN population can be produced under multiple scenarios, select special cases at high redshifts ($z \sim 10$) can only emerge under the most extreme conditions that allow for very efficient accretion and/or heavy-seed formation. Only a subset of SMBHs could have accreted so efficiently, however, as otherwise many more luminous AGN would have been observed at high redshifts beyond the current census.

outlier cases (see below). However, they are in general not necessary to reproduce the $z = 3.5$–5 BHMF, such that the conditions for heavy-seed formation could be more restrictive to reduce their formation and peak height without affecting our overall conclusions.

At $z = 9$–10, we compare our models against select AGN observations at comparable redshifts, UHZ1 at $z = 10.1$ (Á. Bogdán et al. 2024), GHZ9 at $z = 10.145$ (L. Napolitano et al. 2024), and GN-z11 at $z = 10.6$ (R. Maiolino et al. 2024c). As can be seen, under our parameter choices, all Bondi-accretion models roughly match the $z = 3.5$–6 BLAGN BHMF in slope and amplitude, except that the super-Eddington-limited models are slightly above the observations at the highest BH masses. Such overprediction can be mitigated by decreasing the accretion duty cycle, which may be lower for highly accreting objects. Thus, our super-Eddington-limited

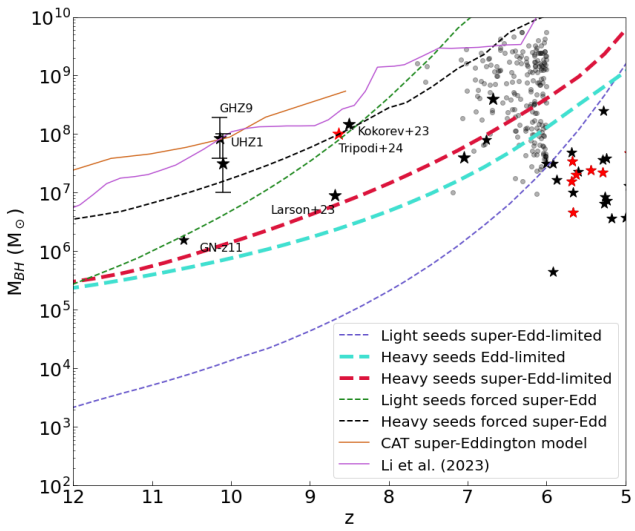

Figure 2. Most massive SMBH vs. redshift for different seeding/growth models with $v_{BC} = 0.8$. We show estimated BH masses for select LRDs (red stars; A. J. Taylor et al. 2025; R. Tripodi et al. 2024), adopting the AGN interpretation. We further plot select JWST-observed high-redshift AGN as black stars (Á. Bogdán et al. 2024; V. Kokorev et al. 2023; R. L. Larson et al. 2023; L. J. Furtak et al. 2024; I. Juodžbalis et al. 2024; R. Maiolino et al. 2024; L. Napolitano et al. 2024), and high-redshift quasars as black dots (R. Wang et al. 2010; C. J. Willott et al. 2017; R. Decarli et al. 2018; T. Izumi et al. 2018; K. Inayoshi et al. 2020; A. Pensabene et al. 2020; S. Fujimoto et al. 2022). We compare our model against the Cosmic Archaeology Tool (CAT) SAM heavy-seed super-Eddington model (R. Schneider et al. 2023), and a heavy-seed model with growth constrained through the quasar luminosity function (W. Li et al. 2024). The highest-redshift ($z \gtrsim 8$) detections can only be reproduced with the forced-Eddington accretion model, whereas the lower-redshift AGN ($z \sim 6$) can also be produced by the Bondi-accretion and Eddington-limited models. To be able to produce the massive UHZ1 object, we include a model with heavy seeds and the forced-Eddington growth model, albeit at a lower duty fraction of 0.5. Therefore, the most massive AGN at the highest redshifts may have formed under the extreme conditions that allowed for continuous Eddington/super-Eddington accretion, while lower-redshift AGN could have formed under more common, less extreme conditions.

models represent somewhat optimistic, but still physically plausible estimates for the BHMF.

Conversely, at $z \sim 10$, only the forced super-Eddington accretion model for light seeds is able to match the upper limit on volume density inferred from UHZ1 (S. Fujimoto et al. 2024). We note that even super-Eddington-limited heavy seeds could not reproduce the inferred UHZ1 abundance at $z \sim 10$. However, the forced super-Eddington model would clearly overproduce the BHMF, compared with the $z = 3.5$–6 observations (D. D. Kocevski et al. 2023; J. Matthee et al. 2024; A. J. Taylor et al. 2025). This model reaches the physical upper limit of accretion, where the BH has accreted all/most of the cold gas available in the halo. In contrast, the volume density inferred for the less massive GN-z11 SMBH can be achieved with heavy seeds. Furthermore, without forced super-Eddington accretion, all light seeds remain below 10^5 $M_\odot$ throughout, and thus cannot produce the observed SMBHs at $z \sim 10$.

3.2. Black Hole Mass Evolution

For each of the models, we further examine the mass of the most massive BH at each redshift and compare it against existing high-redshift quasar and JWST AGN observations. In Figure 2, we show such a comparison. Most models fail to reproduce the most massive AGN observed by JWST at $z \gtrsim 8$, in particular the peculiar UHZ1 and GHZ9 systems, as well as the most massive, high-z quasars, with the exception of the forced-Eddington cases. The latter in turn are close to the "causal limit," where all/most of the cold gas supply in the host halo is accreted. We note that to account for UHZ1, such sustained super-Eddington accretion onto heavy seeds would be required. The extreme accretion and resulting growth of the forced-Eddington models will need to peter out at later times, because if these growth trajectories were to continue, the resulting SMBHs would acquire masses of $\sim 10^{10}$ $M_\odot$ by $z \sim 6$, while such massive objects are extremely rare (X.-B. Wu et al. 2015). This could be explained by the denser environments at higher redshifts that are more suited to enable extreme accretion, whereas gaseous conditions at lower redshifts become less dense and more readily affected by stellar and BH feedback, resulting in less efficient SMBH accretion (e.g., Y. Feng et al. 2014; Y. Ni et al. 2022).

Our findings agree with previous theoretical predictions (M. Volonteri 2010; K. Inayoshi et al. 2020) and SMBH observations prior to JWST (E. Bañados et al. 2018; J. Yang et al. 2021), concluding that to explain the most massive SMBHs in the early Universe, nonstandard pathways such as heavy seeds and/or super-Eddington accretion are required. Our results are further consistent with other theoretical models, such as those obtained within the CAT SAM (R. Schneider et al. 2023), where a heavy seed together with merger-driven super-Eddington accretion was needed to match UHZ1, or the model where a heavy seed with growth constrained through the quasar luminosity function is invoked (W. Li et al. 2024). Overall, the "most massive BH diagnostic" is quite constraining for early seeding and growth models, and the prospect of extending this frontier to even higher redshifts with upcoming, ultradeep JWST observations is compelling. Thus extending the high-redshift frontier may be effectively assisted by gravitational-lensing magnifications, such as with the ongoing GLIMPSE survey (V. Kokorev et al. 2025).

3.3. Overmassive Black Holes

Regarding the coevolution of SMBHs and their host systems, JWST has established the key result that many of the newly discovered sources at high z are overmassive, where the SMBH-to-galaxy stellar mass ratio is much higher than in the local Universe (e.g., R. Maiolino et al. 2024). To explore this complex coevolution within our semianalytical modeling, we show the ratio of BH to stellar mass for the different cases across redshifts in Figure 3. As is evident in the figure, most models can explain the range of observed ratios at $z \lesssim 10$ including the extreme UHZ1 case. This result agrees with previous theoretical studies, including the CAT SAM (A. Trinca et al. 2024), as well as other theoretical models that do not explicitly invoke the heavy-seed formation channel (H. Hu et al. 2025). In fact, while heavy seeds are considered in H. Hu et al. (2025), the BH-to-stellar mass ratios for light and heavy seeds become indistinguishable at the observed redshifts. Similarly, according to the BRAHMA simulations (A. K. Bhowmick et al. 2024b), the details of the heavy-seeding conditions are found to not have a large impact on the resulting distribution of mass ratios. Given the optimistic assumptions in our heavy-seeding model, in terms of their formation and growth, our results should be considered as upper limits for the heavy-seed pathway. When considering all

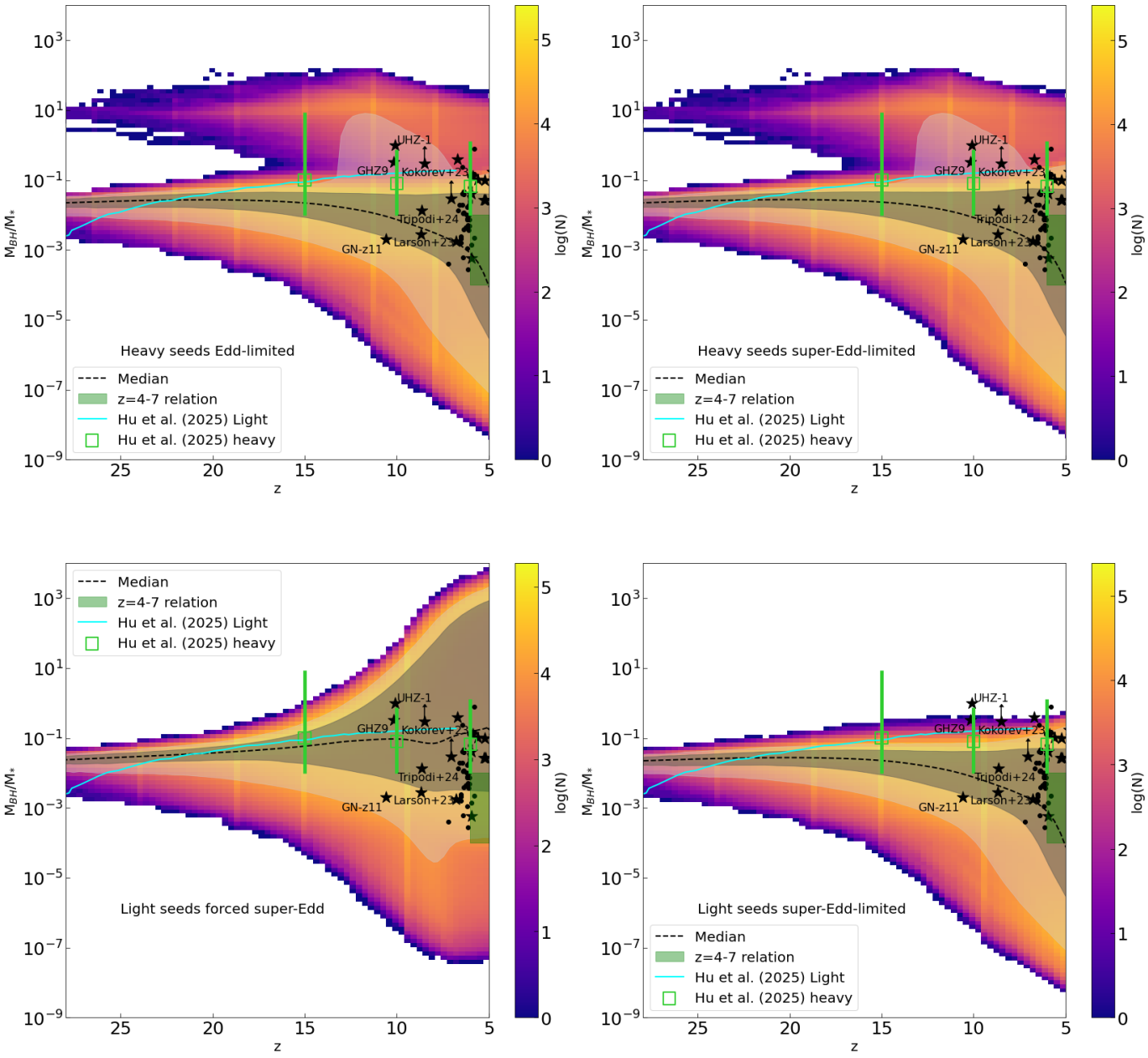

Figure 3. Coevolution of SMBH and its host system. We show the ratio of SMBH to stellar mass vs. redshift, indicating the prevalence of cases (number N) with the given color-coding convention. For each model, we also indicate the median ratio with the black dashed line and the weighted 1σ and 2σ spreads with the ocher green and transparent white shaded regions, respectively. Specifically, all models assume a "standard" value for baryon–DM streaming of $v_{\rm BC} = 0.8$. We further plot select values for JWST-observed, high-redshift AGN as black stars (Á. Bogdán et al. 2024; V. Kokorev et al. 2023; R. L. Larson et al. 2023; L. J. Furtak et al. 2024; I. Juodžbalis et al. 2024; R. Maiolino et al. 2024; L. Napolitano et al. 2024; R. Tripodi et al. 2024), and high-redshift quasars as black dots (R. Wang et al. 2010; C. J. Willott et al. 2017; R. Decarli et al. 2018; T. Izumi et al. 2018; K. Inayoshi et al. 2020; A. Pensabene et al. 2020). For additional context, we reproduce the BH-to-stellar mass relation inferred at $z \sim 4$–7 (F. Pacucci et al. 2023), with the shaded (green) region at the right end of the panels. We compare our results against select heavy- and light-seed models of H. Hu et al. (2025), in which heavy seeds form later. All models produce a wide range of BH-to-stellar mass ratios at $z \lesssim 10$, covering most of the observations. Thus, it will be difficult to distinguish between BH evolutionary pathways, based on the BH-to-stellar mass observations at $z \lesssim 10$ alone. However, clear differences arise at even higher redshifts ($z \gtrsim 15$), to be probed with future ultradeep JWST observations.

seeding channels, heavy seeds represent a small fraction of the overall SMBH population, and only select cases are extremely overmassive as seen in the trend of the median BH-to-stellar mass ratio in Figure 3. Even for models with heavy seeds, the median ratio evolves to lower values at later times. This is in line with existing observations, where few systems are highly overmassive, but many high-redshift AGN exhibit lower $M_{\rm BH}/M^*$ ratios. The notable exception is the light-seed model with (super-Eddington limited) Bondi accretion (bottom-right panel), where typical ratios of $M_{\rm BH}/M_* \sim 10^{-2}$ are established, in line with earlier results that light-seed models cannot efficiently grow, unless sustained periods of super-Eddington accretion can occur (e.g., J. Jeon et al. 2023). We further note that the "light-seeds forced super-Eddington" model produces extremely overmassive systems ($M_{\rm BH}/M_* \sim 10^3$) in large number at $z \sim 5$. However, this model, as stated earlier, is an extreme case and reaches the physical upper limit of accretion, where all available cold gas

is accreted. Therefore, such a model where all seeds grow in this hyperefficient way until lower redshifts ($z \sim 5$) is not plausible. The BHMF is overproduced in this model at lower redshifts as well (Figure 1), further confirming this conclusion. We discuss below that to explain current observations, only a small subset (0.01% at $z \sim 5$–6) of cases could follow such extreme growth trajectories, especially at lower redshifts (See Section 4).

Intriguingly, the near degeneracy of light- and heavy-seed models can be broken when pushing to even higher redshifts. As can be seen, at $z \gtrsim 15$ the heavy-seed models exhibit a bifurcation into two separate branches, overmassive and "normal," at ratios of $\sim$10 and 10^{-2}, respectively. The light-seed growth pathways with forced super-Eddington accretion, on the other hand, initially show a narrow range of BH-to-stellar mass ratios, and only later on, at $z \lesssim 15$ extend into the overmassive domain. If this qualitatively different behavior at high redshifts can be probed with ultradeep JWST surveys, we may have a telltale signature of light versus heavy SMBH seeding. Next, we will further discuss ways to address this key challenge of distinguishing between early seeding and growth channels.

4. Signature of Black Hole Seeding Pathways

From the above results, we conclude that while the observed AGN population and select massive objects at $z \lesssim 8$ can be fairly well described by all our models, there are differences in the most extreme objects the models can produce, as well as the overall amplitude of the BHMF and the location of specific BHMF peaks. We note that larger differences arise at higher redshifts ($z \gtrsim 9$), providing a greater potential to empirically distinguish between models. Specifically, when heavy seeds exist, there is a peak in the mass function at the mass where heavy seeds are initially formed at (10^5 $M_\odot$, for our assumption here), as seen in Figure 1.

Furthermore, under the standard Bondi accretion, the massive SMBHs at $z \sim 10$ with masses larger than 10^5 $M_\odot$ all originate from heavy seeds with no light seeds able to grow that massive at early times. Long periods of efficient super-Eddington accretion, as in our "light-seeds forced super-Eddington" model, are necessary for light seeds to produce such massive cases. We thus confirm that extreme growth may be necessary to produce objects similar to UHZ1.

However, determining which BH seeds could accrete at super-Eddington rates is difficult. Small-scale high-resolution simulations have demonstrated that such extreme conditions are possible (e.g., Y.-F. Jiang et al. 2019a, 2019b; H. Hu et al. 2022; S. T. Gordon et al. 2025; N. Kaaz et al. 2025), but in larger box simulations with lower resolution, such conditions cannot be easily identified. Even more so in this work, we cannot determine which halos experience super-Eddington conditions, since we do not explicitly model the detailed halo gas structure within our semianalytical framework. Therefore, we instead approximately assume that some fraction of all BH seeds will accrete at extreme rates. In Figure 4, we show the BHMF arising from the combination of two modes: forced super-Eddington and (super-)Eddington limited. We attempt to mimic the real Universe with these hybrid models, where most BHs accrete inefficiently represented by the heavy-seeds Eddington-limited model or the light seeds super-Eddington-limited model, while a few exist in environments that allow very efficient accretion as in the case of light seeds forced super-Eddington. At higher redshifts where denser environments are more common, such highly accreting BHs are assumed to be more common as well. Thus, the forced super-Eddington model, assumed to contribute 0.01% of BHs, can reproduce the observed BLAGN BHMF at $z = 5$–6, in combination with and without heavy seeds. At $z = 9$–10, with fewer constraints on the BH population, we consider two contribution values from the efficiently accreting BHs, 0.1% and 1%.

When heavy seeds are included in this combination of models, both the BLAGN BHMF at $z \sim 5$ and the UHZ1 constraint can be reproduced, considering that the latter is an upper limit, and that the actual number density of UHZ1-class systems may be significantly lower. With just light seeds, the earliest AGN systems can only be reproduced when including a fraction of super-Eddington accretion. As before in Figure 1, the key difference when heavy seeds exist is the prominent peak at the heavy-seeding mass. Beyond that, the predicted BHMF slope is very similar at $M_{\rm BH} \gtrsim 10^6$ $M_\odot$ between the two scenarios. The limiting AGN mass allowing detection with current and future JWST surveys (M. Dickinson et al. 2024; K. Kakiichi et al. 2024; S. L. Finkelstein et al. 2025) at $z \sim 9$–10 robustly extends only down to $\sim 10^6$ $M_\odot$. Therefore, based on the BHMF alone, we conclude that future JWST surveys may still not be able to directly distinguish between seeding pathways for the first SMBHs. We compute these estimated AGN BH mass detection limits by simulating JWST observations of BLAGN using the `Pandeia` JWST exposure time calculator engine (K. M. Pontoppidan et al. 2016). We use the relations given in A. E. Reines et al. (2013) to model broad Hα (or broad Hβ at $z > 7$) lines emitted by BLAGN of varying BH mass. We then use `Pandeia` to simulate how these idealized model lines will appear when observed by different JWST programs, and determine—for each program, as a function of redshift—the limiting BH mass at which the broad line can no longer be robustly recovered when fit with Bayesian techniques. We here do not consider the limiting effect of a survey's effective area coverage in observing the most massive AGN, as in the context of this work, we aim to constrain whether these surveys will be able to detect more common and thus less massive SMBHs.

There are, however, promising strategies to work around this conclusion. Gravitational lensing could provide enough flux magnification to enable the discovery of the less massive SMBHs at $\sim 10^5$ $M_\odot$, which are otherwise too faint to be observed (J. Jeon et al. 2023). While gravitational lensing is the only way to probe these low-mass BHs with reasonable integration time on current facilities, the survey volumes of lensed fields are significantly smaller. This effect could be partially offset by the increased number density of faint BHs, but heroic integrations are required to reach these faint sources. One example is the recently approved Director's Discretionary Time follow-up observations of the AS1063 GLIMPSE field (V. Kokorev et al. 2025; S. Fujimoto et al. 2025). With 40 hr integrations and medium spectral resolution, these upcoming observations will be sensitive to BH masses down to 10^5 $M_\odot$, sufficient to provide the first empirical probe of the peak of the BLAGN BHMF due to the DCBH seed mass, although the height of the peak is not fully constrained, subject to the DCBH formation criteria (see Section 3.1).

Alternatively, the fraction/number of highly accreting SMBHs could be well constrained through JWST observations

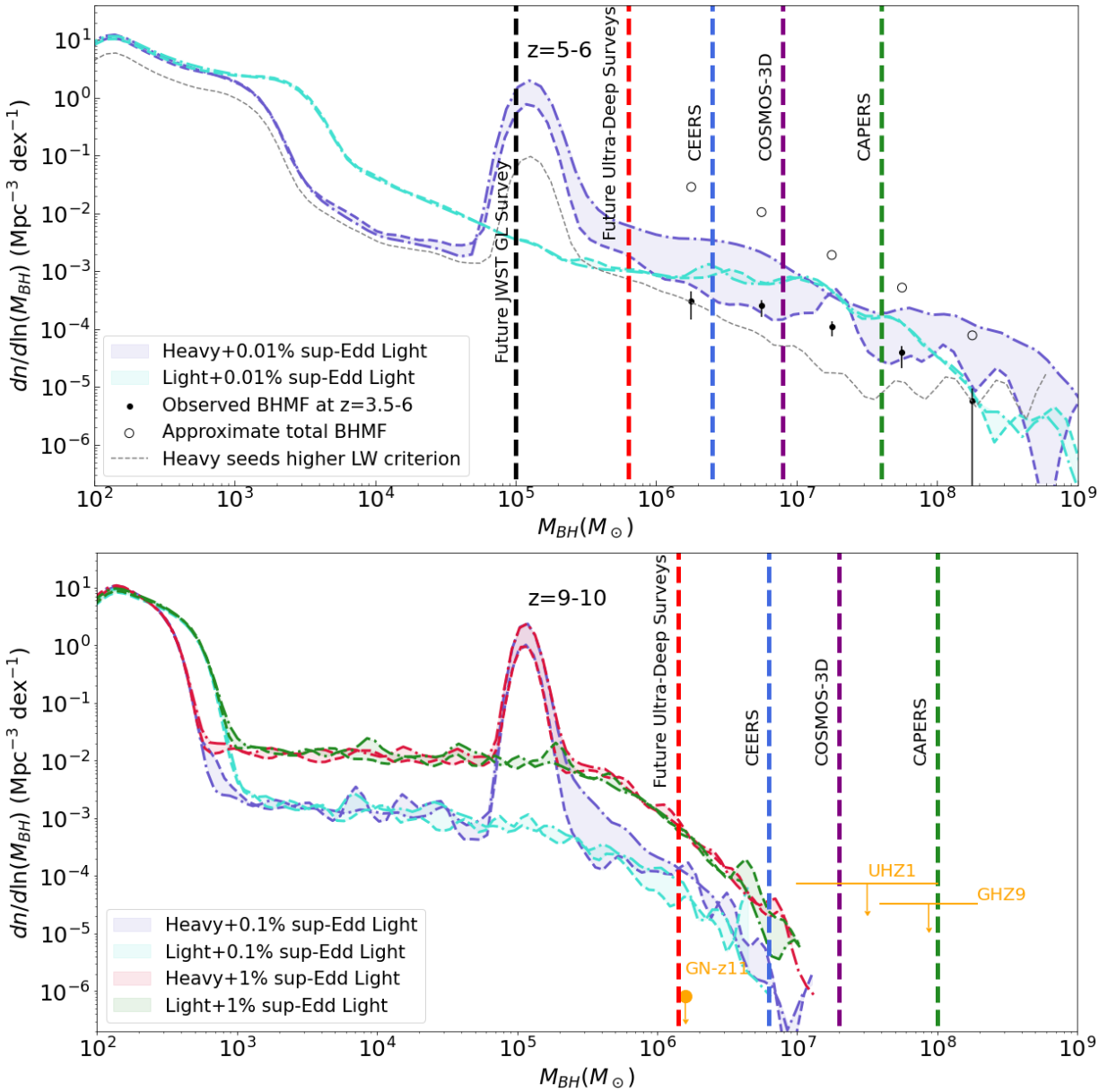

Figure 4. BHMF of various model combinations at $z = 5$–6 and $z = 9$–10, similar to Figure 1. Specifically, we combine the "heavy-seeds Eddington-limited" or "light-seeds super-Eddington-limited" models with a small fraction of "light-seeds forced super-Eddington" model by randomly choosing BHs from each model, with a small probability (0.01%–1%) of choosing the forced super-Eddington BHs. At $z = 5$–6, the super-Eddington fraction is 0.01% to match the observed BHMF, while at $z = 9$–10, we vary the fraction between 0.1% and 1%. The dashed line is the model with $v_{\rm BC} = 0.8$, and the dotted–dashed one the model with the weighted mean of $v_{\rm BC}$ values. The combination of a few BH seeds accreting very efficiently with a majority of seeds accreting at less extreme rates can reproduce all high-redshift observations so far. When heavy seeds are included, a distinctive peak near the DCBH seed mass arises ($10^5\ M_\odot$ for our models), persisting across redshifts ($z \lesssim 15$). JWST gravitational-lensing surveys, such as spectroscopic follow-up to the GLIMPSE survey (H. Atek et al. 2023), could detect such a peak at $z \sim 6$. However, without lensing, current and future JWST surveys such as CEERS (S. L. Finkelstein et al. 2025), COSMOS-3D (K. Kakiichi et al. 2024), and CAPERS (M. Dickinson et al. 2024), will likely not be able to directly detect this DCBH peak, as indicated by their BH mass detection limits, shown with the vertical dashed lines (see Section 4). However, future ultradeep surveys that can probe up to $M_{\rm BH} \sim 10^6\ M_\odot$ at $z \sim 9$ will be able to determine the fraction of highly efficient accreting BHs at higher number densities, up to 2 orders of magnitude than current surveys, resulting in smaller uncertainties. The volume density of the massive AGN sensitively depends on the fraction of high-accreting BHs, such that the number of host halos/galaxies that are able to support such extreme growth could be constrained with near-future observations. The prevalence of heavy seeds could be indirectly constrained as well, if future surveys show a much lower number density than predicted when super-Eddington seeds are included (closer to the limit set by GN-z11), such that the lower number densities predicted for the Eddington-limited heavy-seed scenario would provide a better fit (see also Figure 1).

in the near future. The existing $z \sim 10$ AGN observations are most likely the extremely bright objects in that period. When ultradeep surveys are able to find more such objects at $z \sim 10$, their number density can be constrained with improved accuracy. Moreover, even without gravitational lensing, future ultradeep JWST spectroscopic observations of blank fields could further detect SMBHs at $M_{\rm BH} \sim 10^6\ M_\odot$ via broad Hβ or Hγ observations. As shown from our models in Figure 4, the fraction of highly accreting SMBHs affect the amplitude of the BHMF. If the BHMF at $z \sim 10$ can be constrained at lower BH masses, the fraction of halos/galaxies that can support such highly accreting objects can also be inferred.

It can be argued that the duty fraction we use for the forced super-Eddington model, 0.8, is an extreme value, especially as

super-Eddington SMBHs are expected to have a low duty fraction (E. Pezzulli et al. 2017; F. Fontanot et al. 2023; A. Trinca et al. 2024). However, degeneracy exists between the super-Eddington accretion rate and the accretion duty fraction. The forced super-Eddington rate could be set to a higher value to increase the overall BHMF as well. We have tested decreasing the duty fraction (0.1) but increasing the forced super-Eddington rate (12). The resulting BHMFs were nearly identical to the forced super-Eddington model with no significant differences. This is expected, as in principle, both the duty fraction and the super-Eddington rate work to moderate the accretion rate in our model (see Equations (16) and (18)). Thus, our forced super-Eddington model represents the scenario of extreme BH growth, either through a high duty fraction or extreme super-Eddington accretion. Furthermore, for the forced super-Eddington case, many BHs in the model accrete all available cold gas in the halo, reaching the physical upper limit of accretion.[7] This limit of available gas is a robust limit even when the detailed physical process of BH accretion is not known. Therefore, the super-Eddington fraction we consider here is close to the most optimal SMBH growth, and so our models do show the differences that will exist in the BHMF depending on the fraction of the extreme efficiently accreting SMBHs.

The CEERS survey has already reached the massive end of the BHMF, and can thus begin to measure the highly accreting SMBH fraction. However, CEERS is now completed, yet only a handful of AGN detections at $z \sim 10$ exist, insufficient to constrain this fraction well. As the most massive and brightest SMBHs will be the rarest and lowest in volume density, such a result is not surprising. However, future JWST ultradeep surveys will be able to probe less massive and more abundant SMBHs, up to $\sim$2 orders of magnitude higher in volume density according to our models. Numerous additional AGN are thus expected to be discovered in the near future, and the fraction of efficiently accreting SMBHs will be constrained much more strongly.

Finally, the existence of heavy seeds could be indirectly demonstrated through future surveys. All models summarized in Figure 4 predict values above the upper limit set by the volume density of GN-z11 at $z \sim 10$. This could be due to observational incompleteness, missing fainter or obscured AGN. However, if future observations were to show that the SMBH BHMF is closer to the GN-z11 value, this would indicate that very few SMBHs would experience efficient growth at (sustained) super-Eddington levels. Similar conclusions could be drawn if the current high upper limit for the abundance of UHZ1-type systems would be revised downwards. Since light seeds without extended super-Eddington growth cannot reach masses as high as the GN-z11 SMBH at $z \sim 10$, and if observations were to confirm the low abundance estimate in this mass range, a heavy-seed origin would be favored. UHZ1 and GHZ9 in this case would be extreme outliers, which may require heavy DCBH seeds, possibly combined with efficient super-Eddington growth episodes. Other theoretical models like TRINITY, constrained with high-redshift UV luminosity functions, could not reproduce a system like UHZ1 and have also found it to be an outlier case (H. Zhang et al. 2023). The constraints on such extreme and massive SMBHs will be rendered much stronger with the Nancy Grace Roman Space Telescope telescope, which is expected to find massive quasars at $z \sim$ 6–10 (H. Zhang et al. 2024).

[7] We have estimated in postprocessing the Bondi–Hoyle boost factor, α, that would be needed to reproduce the forced-Eddington accretion rates. For the top 25% most massive SMBHs, equivalent boost factors would be $\sim 10^3$–10^4. Thus, the forced-Eddington model probes the extreme upper limit of BH growth.

5. Summary and Conclusions

In this work, we have modified the SAM A-SLOTH to include the seeding and evolution of the first SMBHs in the Universe. We explore various seeding and accretion scenarios, including heavy DCBH seeds, light stellar remnant seeds, Bondi–Hoyle accretion, and enforced super-Eddington accretion. We find that, even with differences in the BHMF features and overall amplitude, the observed BLAGN BHMF at $z = 3.5$–6 can be largely reproduced with a broad selection of models and their parameters, albeit with considerable degeneracies between them, similar to constraints from more local BHMF determinations (A. E. Evans et al. 2025).

To possibly break this degeneracy, we examine our models at higher redshifts, $z \sim$ 9–10, and find that although existing and near-future JWST surveys may still not be able to directly identify the dominant SMBH seeding scenario, powerful empirical constraints can be obtained. Both seeding models are able to produce the massive AGN and overmassive systems observed at high redshifts, either through having higher mass initially (heavy seeds) or accreting efficiently at super-Eddington rates (light seeds). A key target for the next cycles of JWST observations is to constrain the SMBH accretion mode, as they will preferentially discover the extremely high-accreting AGN. The amplitude of the BHMF will change according to the number of efficiently accreting AGN, which are the main sources for the extreme objects currently being observed at $z \sim 10$, whether they originate from heavy or light seeds. Future ultradeep surveys with JWST will be able to observe SMBHs with masses as low as $\sim 10^6\ M_\odot$, which are predicted to be around 2 orders of magnitude more abundant than currently observable SMBHs so that their super-Eddington fraction will be much better constrained.

Furthermore, the existence of heavy DCBH seeds could be indirectly confirmed through observations of SMBH-to-stellar mass ratios at $z \gtrsim 15$ or if the observed BHMF at mass ranges around $10^6\ M_\odot$ in future surveys exhibits lower abundances than predicted when a super-Eddington accretion mode is included. Put differently, any prevalence of (sustained) super-Eddington accretion modes would drive up the number densities of massive SMBHs, because such efficient accretion would boost a significant fraction of the abundant light seeds into the observable regime. Conversely, without super-Eddington accretion, only heavy seeds can reach high enough masses to be observable by $z \sim 10$, so that a low BHMF amplitude observation will imply that the observed SMBHs originated from heavy seeds. The existence of heavy seeds could even be directly confirmed through JWST gravitational-lensing surveys. In addition, different pathways for heavy-seed formation could leave different observational signatures (A. K. Bhowmick et al. 2025), as we have only tested one heavy-seed formation mechanism in this work.

Finally, complementary future multiwavelength and multi-messenger observations could further elucidate SMBH seeding pathways. PTA observations have detected the stochastic GWB (G. Agazie et al. 2023a; EPTA Collaboration et al. 2023;

D. J. Reardon et al. 2023; H. Xu et al. 2023), which if sourced from binary SMBHs (G. Hobbs & S. Dai 2017; J. D. Romano & N. J. Cornish 2017), could be used to constrain their population at high redshifts. Future GW observatories like LISA will be able to more robustly detect such signals (T. Robson et al. 2019). Furthermore, future X-ray missions could detect additional AGN at earlier times, targeting sources which may be too X-ray weak to be detected currently (I. Juodžbalis et al. 2023; D. D. Kocevski et al. 2025; M. Yue et al. 2024). For example, the Athena mission will be able to detect much fainter AGN than currently possible with existing optical and near-IR surveys (D. Barret et al. 2013), and the AXIS mission will discover SMBHs with masses below $10^5\ M_\odot$ to probe SMBH seeding pathways (C. S. Reynolds et al. 2023; N. Cappelluti et al. 2024). In the long-term future, the Lynx X-ray mission aims to detect the first BH seeds with a 100 times increase in X-ray sensitivity compared to the Chandra observatory (J. A. Gaskin et al. 2019). Therefore, with JWST observations charting the broad outlines of the first SMBHs and their evolutionary pathways, future observatories will be able to follow up in greater depth, thus completing our understanding of how the Universe has created these massive objects so early in its history.

Acknowledgments

The authors acknowledge the Texas Advanced Computing Center (TACC) for providing HPC resources under FRONTERA allocation AST22003. B.L. gratefully acknowledges the funding of the Royal Society University Research Fellowship and the Deutsche Forschungsgemeinschaft (DFG, German Research Foundation) under Germany's Excellence Strategy EXC 2181/1—390900948 (the Heidelberg STRUCTURES Excellence Cluster). A.J.T. acknowledges support from the UT Austin College of Natural Sciences.

ORCID iDs

Junehyoung Jeon https://orcid.org/0000-0002-6038-5016
Boyuan Liu https://orcid.org/0000-0002-4966-7450
Anthony J. Taylor https://orcid.org/0000-0003-1282-7454
Vasily Kokorev https://orcid.org/0000-0002-5588-9156
John Chisholm https://orcid.org/0000-0002-0302-2577
Dale D. Kocevski https://orcid.org/0000-0002-8360-3880
Steven L. Finkelstein https://orcid.org/0000-0001-8519-1130
Volker Bromm https://orcid.org/0000-0003-0212-2979

References

Agazie, G., Anumarlapudi, A., Archibald, A. M., et al. 2023a, ApJL, 951, L8
Agazie, G., Anumarlapudi, A., Archibald, A. M., et al. 2023b, ApJL, 952, L37
Agazie, G., Anumarlapudi, A., Archibald, A. M., et al. 2023c, ApJL, 951, L50
Akins, H. B., Casey, C. M., Lambrides, E., et al. 2024, arXiv:2406.10341
Arca-Sedda, M. 2016, MNRAS, 455, 35
Arca-Sedda, M., Capuzzo-Dolcetta, R., Antonini, F., & Seth, A. 2015, ApJ, 806, 220
Ardaneh, K., Luo, Y., Shlosman, I., et al. 2018, MNRAS, 479, 2277
Askar, A., Baldassare, V. F., & Mezcua, M. 2023, arXiv:2311.12118
Atek, H., Chisholm, J., Alavi, A., et al. 2023, JWST Proposal. Cycle 2, ID., #3293
Bañados, E., Venemans, B. P., Mazzucchelli, C., et al. 2018, Natur, 553, 473
Baggen, J. F. W., van Dokkum, P., Brammer, G., et al. 2024, ApJL, 977, L13
Barret, D., Nandra, K., Barcons, X., et al. 2013, in SF2A-2013: Proc. Annual meeting of the French Society of Astronomy and Astrophysics ed. L. Cambresy et al. (Paris: Société Francaise d'Astronomie et d'Astrophysique - SF2A), 447
Becerra, F., Marinacci, F., Bromm, V., & Hernquist, L. E. 2018a, MNRAS, 480, 5029
Becerra, F., Marinacci, F., Inayoshi, K., Bromm, V., & Hernquist, L. E. 2018b, ApJ, 857, 138
Begelman, M. C. 1979, MNRAS, 187, 237
Begelman, M. C., Volonteri, M., & Rees, M. J. 2006, MNRAS, 370, 289
Beifiori, A., Courteau, S., Corsini, E. M., & Zhu, Y. 2012, MNRAS, 419, 2497
Bhowmick, A. K., Blecha, L., Torrey, P., et al. 2024a, MNRAS, 529, 3768
Bhowmick, A. K., Blecha, L., Torrey, P., et al. 2024b, MNRAS, 533, 1907
Bhowmick, A. K., Blecha, L., Torrey, P., et al. 2025, MNRAS, 538, 518
Binney, J., & Tremaine, S. 2008, Galactic Dynamics: Second Edition (Princeton, NJ: Princeton Univ. Press)
Bogdán, Á., Goulding, A. D., Natarajan, P., et al. 2024, NatAs, 8, 126
Bondi, H., & Hoyle, F. 1944, MNRAS, 104, 273
Bosman, S. E. I., Álvarez-Márquez, J., Colina, L., et al. 2024, NatAs, 8, 1054
Bromm, V., & Loeb, A. 2003, ApJ, 596, 34
Cappelluti, N., Foord, A., Marchesi, S., et al. 2024, Univ, 10, 2 76
Chen, L.-H., Magg, M., Hartwig, T., et al. 2022, MNRAS, 513, 934
Chen, N., Mukherjee, D., Matteo, T. D., et al. 2024, OJAp, 7, 28
Chiaki, G., Tominaga, N., & Nozawa, T. 2017, MNRAS, 472, L115
Chon, S., Hirano, S., Hosokawa, T., & Yoshida, N. 2016, ApJ, 832, 134
Chon, S., Hosokawa, T., & Omukai, K. 2021, MNRAS, 502, 700
Chon, S., & Omukai, K. 2025, MNRAS, 539, 2561
Correa, C. A., Wyithe, J. S. B., Schaye, J., & Duffy, A. R. 2015, MNRAS, 452, 1217
Croton, D. J. 2006, MNRAS, 369, 1808
Davis, S. W., & Tchekhovskoy, A. 2020, ARA&A, 58, 407
Decarli, R., Walter, F., Venemans, B. P., et al. 2018, ApJ, 854, 97
Deng, Y., Li, H., Liu, B., et al. 2024, A&A, 691, A231
Dickinson, M., Amorin, R., Arrabal Haro, P., et al. 2024, JWST Proposal. Cycle 3 ID., #6368
Diemer, B. 2018, ApJS, 239, 35
Ding, X., Silverman, J., Treu, T., et al. 2020, ApJ, 888, 37
Ding, X., Silverman, J. D., & Onoue, M. 2022, ApJL, 939, L28
Durodola, E., Pacucci, F., & Hickox, R. C. 2025, ApJ, 985, 169
EPTA CollaborationInPTA Collaboration, Antoniadis, J., et al. 2023, A&A, 678, A50
Evans, A. E., Blecha, L., & Bhowmick, A. K. 2025, MNRAS, 536, 2783
Fan, X., Bañados, E., & Simcoe, R. A. 2023, ARA&A, 61, 373
Feng, Y., Di Matteo, T., Croft, R., & Khandai, N. 2014, MNRAS, 440, 1865
Finkelstein, S. L., Bagley, M. B., Arrabal Haro, P., et al. 2025, ApJ, 983, 4
Fontanot, F., Cristiani, S., Grazian, A., et al. 2023, MNRAS, 520, 740
Fujimoto, S., Brammer, G. B., Watson, D., et al. 2022, Natur, 604, 261
Fujimoto, S., Naidu, R. P., Chisholm, J., et al. 2025, arXiv:2501.11678
Fujimoto, S., Wang, B., Weaver, J. R., et al. 2024, ApJ, 977, 250
Furtak, L. J., Labbé, I., Zitrin, A., et al. 2024, Natur, 628, 57
Gaete, B., Schleicher, D. R. G., Lupi, A., et al. 2024, A&A, 690, A378
Gaskin, J. A., Swartz, D. A., Vikhlinin, A., et al. 2019, JATIS, 5, 021001
Gebhardt, K., Bender, R., Bower, G., et al. 2000, ApJL, 539, L13
Gordon, S. T., Smith, B. D., Khochfar, S., & Beckmann, R. S. 2025, MNRAS, 537, 674
Graham, A. W., Onken, C. A., Athanassoula, E., & Combes, F. 2011, MNRAS, 412, 2211
Greene, J. E., Labbe, I., Goulding, A. D., et al. 2024, ApJ, 964, 39
Greene, J. E., Strader, J., & Ho, L. C. 2020, AR&A, 58, 257
Greif, T. H., & Bromm, V. 2006, MNRAS, 373, 128
Guia, C. A., Pacucci, F., & Kocevski, D. D. 2024, RNAAS, 8, 207
Haemmerlé, L., Mayer, L., Klessen, R. S., et al. 2020, SSRv, 216, 48
Haemmerlé, L., Woods, T. E., Klessen, R. S., Heger, A., & Whalen, D. J. 2018, MNRAS, 474, 2757
Haiman, Z., & Loeb, A. 2001, ApJ, 552, 459
Hartwig, T., Lipatova, V., Glover, S. C. O., & Klessen, R. S. 2024, MNRAS, 535, 516
Hartwig, T., Magg, M., Chen, L.-H., et al. 2022, ApJ, 936, 45
Heckman, T. M., & Best, P. N. 2014, ARA&A, 52, 589
Heger, A., Fryer, C. L., Woosley, S. E., Langer, N., & Hartmann, D. H. 2003, ApJ, 591, 288
Hickox, R. C., & Alexander, D. M. 2018, ARA&A, 56, 625
Hirano, S., & Bromm, V. 2017, MNRAS, 470, 898
Hobbs, G., & Dai, S. 2017, NSRev, 4, 707
Hu, H., Inayoshi, K., Haiman, Z., Ho, L. C., & Ohsuga, K. 2025, ApJ, 983, 37

Hu, H., Inayoshi, K., Haiman, Z., Quataert, E., & Kuiper, R. 2022, ApJ, 934, 132
Huang, H.-L., Jiang, J.-Q., He, J., Wang, Y.-T., & Piao, Y.-S. 2024, arXiv:2410.20663
Inayoshi, K. 2025, arXiv:2503.05537
Inayoshi, K., Kimura, S., & Noda, H. 2024, arXiv:2412.03653
Inayoshi, K., & Tanaka, T. L. 2015, MNRAS, 450, 4350
Inayoshi, K., Visbal, E., & Haiman, Z. 2020, ARA&A, 58, 27
Izumi, T., Onoue, M., Shirakata, H., et al. 2018, PASJ, 70, 36
Jeon, J., Bromm, V., & Finkelstein, S. L. 2022, MNRAS, 515, 5568
Jeon, J., Bromm, V., Liu, B., & Finkelstein, S. L. 2025, ApJ, 979, 127
Jeon, J., Liu, B., Bromm, V., & Finkelstein, S. L. 2023, MNRAS, 524, 176
Jeon, M., Pawlik, A. H., Greif, T. H., et al. 2012, ApJ, 754, 34
Jiang, Y.-F., Blaes, O., Stone, J. M., & Davis, S. W. 2019a, ApJ, 885, 144
Jiang, Y.-F., Stone, J. M., & Davis, S. W. 2014, ApJ, 796, 106
Jiang, Y.-F., Stone, J. M., & Davis, S. W. 2019b, ApJ, 880, 67
Johnson, J. L., & Bromm, V. 2007, MNRAS, 374, 1557
Johnson, J. L., Whalen, D. J., Li, H., & Holz, D. E. 2013, ApJ, 771, 116
Juodžbalis, I., Conselice, C. J., Singh, M., et al. 2023, MNRAS, 525, 1353
Juodžbalis, I., Maiolino, R., Baker, W. M., et al. 2024, Natur, 636, 594
Kaaz, N., Liska, M., Tchekhovskoy, A., Hopkins, P. F., & Jacquemin-Ide, J. 2025, ApJ, 979, 248
Kakiichi, K., Egami, E., Fan, X., et al. 2024, JWST Proposal. Cycle 3 ID., #5893
King, A. 2025, MNRAS, 536, L1
Klessen, R. S., & Glover, S. C. O. 2023, ARA&A, 61, 65
Kobayashi, C., Umeda, H., Nomoto, K., Tominaga, N., & Ohkubo, T. 2006, ApJ, 653, 1145
Kocevski, D. D., Finkelstein, S. L., Barro, G., et al. 2025, ApJ, 986, 126
Kokorev, V., Fujimoto, S., Labbe, I., et al. 2023, ApJL, 957, L7
Kocevski, D. D., Onoue, M., Inayoshi, K., et al. 2023, ApJL, 954, L4
Kokorev, V., Atek, H., Chisholm, J., et al. 2025, ApJL, 983, L22
Kokorev, V., Chisholm, J., Endsley, R., et al. 2024, ApJ, 975, 178
Kormendy, J., & Ho, L. C. 2013, ARA&A, 51, 511
Kroupa, P. 2001, MNRAS, 322, 231
Lai, S., Onken, C. A., Wolf, C., Bian, F., & Fan, X. 2024, MNRAS, 531, 2245
Larson, R. L., Finkelstein, S. L., Kocevski, D. D., et al. 2023, ApJL, 953, L29
Latif, M. A., Whalen, D., & Khochfar, S. 2022, ApJ, 925, 28
Leung, G. C. K., Finkelstein, S. L., Pérez-González, P. G., et al. 2024, arXiv:2411.12005
Li, W., Inayoshi, K., Onoue, M., et al. 2024, ApJ, 969, 69
Li, Y., Hernquist, L., Robertson, B., et al. 2007, ApJ, 665, 187
Liu, B., & Bromm, V. 2020a, MNRAS, 495, 2475
Liu, B., & Bromm, V. 2020b, MNRAS, 497, 2839
Liu, B., & Bromm, V. 2022, ApJL, 937, L30
Liu, B., & Bromm, V. 2023, arXiv:2312.04085
Liu, B., Gurian, J., Inayoshi, K., et al. 2024a, MNRAS, 534, 290
Liu, B., Hartwig, T., Sartorio, N. S., et al. 2024b, MNRAS, 534, 1634
Lodato, G., & Natarajan, P. 2006, MNRAS, 371, 1813
Lodato, G., & Natarajan, P. 2007, MNRAS, 377, L64
Luo, Y., Shlosman, I., Nagamine, K., & Fang, T. 2020, MNRAS, 492, 4917
Madau, P., & Haardt, F. 2024, ApJL, 976, L24
Madau, P., & Rees, M. J. 2001, ApJL, 551, L27
Magg, M., Hartwig, T., Chen, L.-H., & Tarumi, Y. 2022, JOSS, 7, 4417
Magg, M., Hartwig, T., Glover, S. C. O., Klessen, R. S., & Whalen, D. J. 2016, MNRAS, 462, 3591
Maiolino, R., Risaliti, G., Signorini, M., et al. 2025, MNRAS, 538, 1921
Maiolino, R., Scholtz, J., Curtis-Lake, E., et al. 2024, A&A, 691, A145
Maiolino, R., Scholtz, J., Witstok, J., et al. 2024c, Natur, 627, 59
Marconi, A., Risaliti, G., Gilli, R., et al. 2004, MNRAS, 351, 169
Matthee, J., Naidu, R. P., Brammer, G., et al. 2024, ApJ, 963, 129
Mezcua, M., & Domínguez Sánchez, H. 2020, ApJL, 898, L30
Milosavljević, M., Couch, S. M., & Bromm, V. 2009, ApJL, 696, L146
Napolitano, L., Castellano, M., Pentericci, L., et al. 2024, arXiv:2410.18763
Natarajan, P., Pacucci, F., Ricarte, A., et al. 2024, ApJL, 960, L1
Navarro, J. F., Frenk, C. S., & White, S. D. M. 1996, ApJ, 462, 563
Ni, Y., Di Matteo, T., & Feng, Y. 2022, MNRAS, 509, 3043
Nomoto, K., Kobayashi, C., & Tominaga, N. 2013, ARA&A, 51, 457
Ogata, E., Ohsuga, K., Fukushima, H., & Yajima, H. 2024, MNRAS, 528, 2588
Oio, G. A., Dai, Y. S., Bornancini, C. G., & Li, Z.-J. 2024, ApJ, 962, 146
Onoue, M., Inayoshi, K., Ding, X., et al. 2023, ApJL, 942, L17
Pacucci, F., & Narayan, R. 2024, ApJ, 976, 96
Pacucci, F., Nguyen, B., Carniani, S., Maiolino, R., & Fan, X. 2023, ApJL, 957, L3
Parkinson, H., Cole, S., & Helly, J. 2008, MNRAS, 383, 557
Partmann, C., Naab, T., Lahén, N., et al. 2025, MNRAS, 537, 956
Pensabene, A., Carniani, S., Perna, M., et al. 2020, A&A, 637, A84
Pérez-González, P. G., Barro, G., Rieke, G. H., et al. 2024, ApJ, 968, 4
Pezzulli, E., Volonteri, M., Schneider, R., & Valiante, R. 2017, MNRAS, 471, 589
Pontoppidan, K. M., Pickering, T. E., Laidler, V. G., et al. 2016, Proc. SPIE, 9910, 991016
Porras-Valverde, A. J., Ricarte, A., Natarajan, P., et al. 2025, arXiv:2504.11566
Reardon, D. J., Zic, A., Shannon, R. M., et al. 2023, ApJL, 951, L6
Regan, J., & Volonteri, M. 2024, OJAp, 7, 72
Reines, A. E., Condon, J. J., Darling, J., & Greene, J. E. 2020, ApJ, 888, 36
Reines, A. E., Greene, J. E., & Geha, M. 2013, ApJ, 775, 116
Reinoso, B., Klessen, R. S., Schleicher, D., Glover, S. C. O., & Solar, P. 2023, MNRAS, 521, 3553
Reynolds, C. S., Kara, E. A., Mushotzky, R. F., et al. 2023, Proc. SPIE, 12678, 126781e
Robson, T., Cornish, N. J., & Liu, C. 2019, CQGra, 36, 105011
Romano, J. D., & Cornish, N. J. 2017, LRR, 20, 2
Safarzadeh, M., & Haiman, Z. 2020, ApJL, 903, L21
Safranek-Shrader, C., Montgomery, M. H., Milosavljević, M., & Bromm, V. 2016, MNRAS, 455, 3288
Sassano, F., Schneider, R., Valiante, R., et al. 2021, MNRAS, 506, 613
Schaerer, D. 2002, A&A, 382, 28
Schauer, A. T. P., Glover, S. C. O., Klessen, R. S., & Clark, P. 2021, MNRAS, 507, 1775
Schauer, A. T. P., Liu, B., & Bromm, V. 2019, ApJ, 877, L5
Schneider, R., Valiante, R., Trinca, A., et al. 2023, MNRAS, 526, 3250
Scholtz, J., Maiolino, R., D'Eugenio, F., et al. 2025, A&A, 697, A175
Sheth, R. K., Mo, H. J., & Tormen, G. 2001, MNRAS, 323, 1
Silk, J., Begelman, M. C., Norman, C., Nusser, A., & Wyse, R. F. G. 2024, ApJL, 961, L39
Smith, A., & Bromm, V. 2019, ConPh, 60, 111
Smith, B. D., Regan, J. A., Downes, T. P., et al. 2018, MNRAS, 480, 3762
Spitzer, L. 1978, Physical Processes in the Interstellar Medium (New York: Wiley)
Stacy, A., Bromm, V., & Lee, A. T. 2016, MNRAS, 462, 1307
Stahler, S. W., & Palla, F. 2004, The Formation of Stars (New York: Wiley)
Sugimura, K., Omukai, K., & Inoue, A. K. 2014, MNRAS, 445, 544
Sullivan, J., Haiman, Z., Kulkarni, M., & Visbal, E. 2025, arXiv:2501.12986
Suresh, A., & Blanton, M. R. 2024, ApJ, 977, 194
Taylor, A. J., Finkelstein, S. L., Kocevski, D. D., et al. 2025, ApJ, 986, 165
Tremmel, M., Karcher, M., Governato, F., et al. 2017, MNRAS, 470, 1121
Treu, T., Roberts-Borsani, G., Bradac, M., et al. 2022, ApJ, 935, 110
Trinca, A., Schneider, R., Valiante, R., et al. 2022, MNRAS, 511, 616
Trinca, A., Valiante, R., Schneider, R., et al. 2024, arXiv:2412.14248
Tripodi, R., Martis, N., Markov, V., et al. 2024, arXiv:2412.04983
Volonteri, M. 2010, A&ARv, 18, 279
Volonteri, M., Habouzit, M., & Colpi, M. 2021, NatRP, 3, 732
Wang, R., Carilli, C. L., Neri, R., et al. 2010, ApJ, 714, 699
Willott, C. J., Bergeron, J., & Omont, A. 2017, ApJ, 850, 108
Wise, J. H., Regan, J. A., O'Shea, B. W., et al. 2019, Natur, 566, 85
Woods, T. E., Agarwal, B., Bromm, V., et al. 2019, PASA, 36, e027
Wu, X.-B., Wang, F., Fan, X., et al. 2015, Natur, 518, 512
Xu, H., Chen, S., Guo, Y., et al. 2023, RAA, 23, 075024
Yang, J., Wang, F., Fan, X., et al. 2021, ApJ, 923, 262
Yue, M., Eilers, A.-C., Simcoe, R. A., et al. 2024, ApJ, 966, 176
Zhang, H., Behroozi, P., Volonteri, M., et al. 2023, MNRAS, 518, 2123
Zhang, H., Behroozi, P., Volonteri, M., et al. 2024, MNRAS, 531, 4974
Zubovas, K., & King, A. 2021, MNRAS, 501, 4289
Zwick, L., Mayer, L., Haemmerlé, L., & Klessen, R. S. 2023, MNRAS, 518, 2076